



MOX–Report No. 25/2011

**Finite element analysis for a multi-mechanism damage
model of cerebral arterial tissue**

DE LUCA, M.; AMBROSI, D.; ROBERTSON, A.M.;
VENEZIANI, A.; QUARTERONI, A.

MOX, Dipartimento di Matematica “F. Brioschi”
Politecnico di Milano, Via Bonardi 9 - 20133 Milano (Italy)

mox@mate.polimi.it

<http://mox.polimi.it>

Finite Element analysis for a multi-mechanism damage model of cerebral arterial tissue*

M. de Luca [‡], D. Ambrosi [‡], A. M. Robertson [†], A. Veneziani [‡], A. Quarteroni^{‡§}

April 27, 2010

[‡] Dipartimento di Matematica “F. Brioschi”
Politecnico di Milano
via Bonardi 9, 20133 Milano, Italy

[†] Department of Mechanical Engineering and Materials Science
University of Pittsburgh
648 Benedum Hall
3700 O’Hara Street, Pittsburgh, PA 15261

[‡] Department of Mathematics and Computer Science
Emory University
400 Dowman Dr, 30322 Atlanta, GA, USA

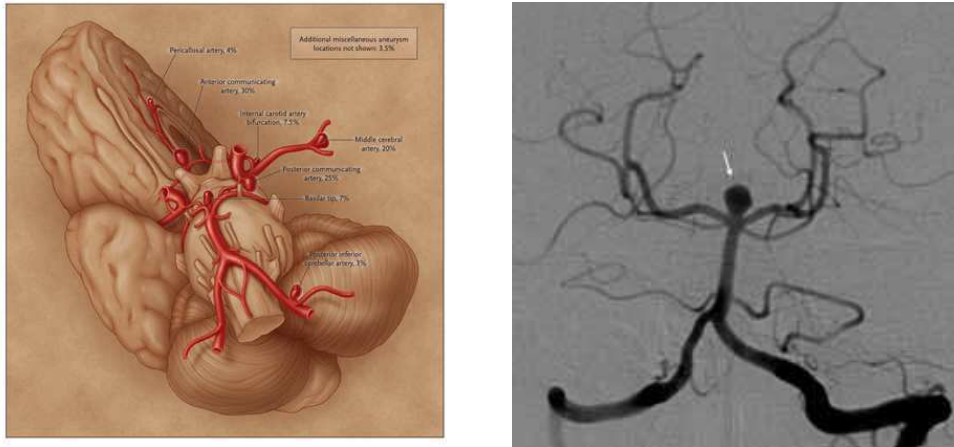
[§] Mathematics Institute of Computational Science and Engineering
Ecole Polytechnique Federale de Lausanne
Bat. MA, Av. Piccard, Station 8, CH-1015 Lausanne (Switzerland)

Abstract

We developed a non-linear multi-mechanism model, that is suitable to represent the mechanical behavior of the healthy arterial wall and the early stage cerebral aneurysm formation. A cerebral aneurysm is a localized bulge of the arterial wall, resulting from an initial dilatation.

The core of the multi-mechanism model is to consider the arterial wall made up of two mechanisms, related to its two main passive constituents: elastin and collagen. Histological studies show that the early stage aneurysm formation is associated with the disruption of elastin, that is found fragmented in the arterial wall. From experimental observations, the elastin actively contributes to load bearing even at low deformation levels, while the collagen network is in a crimped state in its stress-free configuration. For larger deformations, the collagen network stretches out and starts to contribute to the mechanical behavior of the arterial wall. The strain energy of the model is additively composed of two terms, one related to the first mechanism and the other related to the second

*This work has been supported by the ERC Advanced Grant N.227058 MATHCARD



(a) Draw of the circle of willis with some aneurysms [1].

(b) Clinical angiography image of an aneurysm at the apex of the basilar artery [2].

FIGURE 1: Graphic representation and clinical image of cerebral aneurysms.

one. The collagen recruitment happens when a threshold deformation is reached. In our model this threshold is checked at each time step in each element of the computational domain allowing a non-uniform collagen activation across the material. The fragmentation of elastin is modeled by multiplying the stress tensor term related to the first mechanism by a suitable damage coefficient. The latter gradually decreases from one (first mechanism active) to zero (disappearance of first mechanism) as function of deformation.

Our model has been implemented in a FE code that has been validated on a set of test cases for which an analytical solution is available, showing the expected behavior. Numerical simulations for more realistic geometries have shown that the computational multi-mechanism model is able to capture the non-linearity and inelasticity of the arterial wall, as well as early stage aneurysm formation.

keywords: Cerebral aneurysm, Cerebral arteries, Multi-mechanism model, Weakly compressible materials, Finite element analysis, Continuous damage.

1 Introduction to cerebral aneurysms

A *cerebral aneurysm* (also known as intracranial or intracerebral aneurysm) is an abnormal localized dilation of a cerebral artery, filled with blood (figure 1(a) and 1(b)). Usually, it is asymptomatic until rupture. When rupture occurs, the aneurysm leaks or spills blood in the subarachnoid space in the brain, causing the so-called *subarachnoid hemorrhage* [3]. This hemorrhage is potentially lethal

with a mortality rate as high as 50%. Many patients who survive have permanent disability. Some aneurysms reveal their presence before rupture by exerting pressure on a nerve or on the surrounding brain tissue. Usually that happens when the aneurysm is localized in the posterior cerebral circulation. Cerebral aneurysms can occur anywhere in the brain, but usually they are located on, or close to, the *Circle of Willis* [4], between the underside of the brain and the base of the skull. No method is yet known to prevent the formation of a cerebral aneurysm. The difference between a healthy and a pathological artery is based on the knowledge of the morphological structure of the arterial wall.

1.1 Histology of cerebral arteries and aneurysm wall

In this work we focus on the passive behavior of arteries, that is the mechanical stress-strain relation of its own material seen as an inert material: remodelling issues are neglected. From the structural point of view, the arterial wall is composed of three distinct layers, the *tunica intima*, the *tunica media* and the *tunica externa (adventitia)*. In figure 2 there is a schematic representation of the components of a healthy arterial wall.

The intima is the innermost layer of the artery. It consists mainly of a single layer of endothelial cells. In healthy young individuals, the intima is very thin and provides a minor contribution to the mechanical properties of the arterial wall. However, the intima thickens and stiffens with age (*arteriosclerosis*), hence the mechanical contribution may become relevant. Pathological changes of the intimal components may be associated with *atherosclerosis*, the most common disease of the arterial wall. It consists in deposition of material, such as calcium, cellular waste products, and fibrin, that in a healthy situation are carried away by the blood flow. The resulting build-up is called *atherosclerotic plaque*. It may be very complex in geometry and biochemical composition. The presence of this pathological structure causes significant alterations in the mechanical behavior of the arterial wall [5].

The media is the middle layer of an artery and it is composed of a complex three-dimensional network of smooth muscle cells, elastin and collagen fibrils. Elastic layers, called fenestrated *elastic laminae*, separate the media into a varying number of well-defined concentrically fiber reinforced layers [6]. The number of elastic laminae decreases toward the peripheral circulation. The media is separated from the intima and the adventitia by the *internal elastic lamina* (IEL) and the *external elastic lamina* (EEL), respectively. In small vessels, and in particular in cerebral arteries, the EEL is poorly developed [7].

The adventitia, the outermost layer of an artery, is mainly made of collagen, fibroblasts, and fibrocytes, which are cells that mainly produce collagen. The adventitia is surrounded by connective tissue. The thickness of the adventitia strongly depends on the artery type. In particular, in cerebral arteries this constitutive layer is almost absent [7]. Close to the bifurcations, the media tapers gradually. At the bifurcations, the tunica media is completely replaced

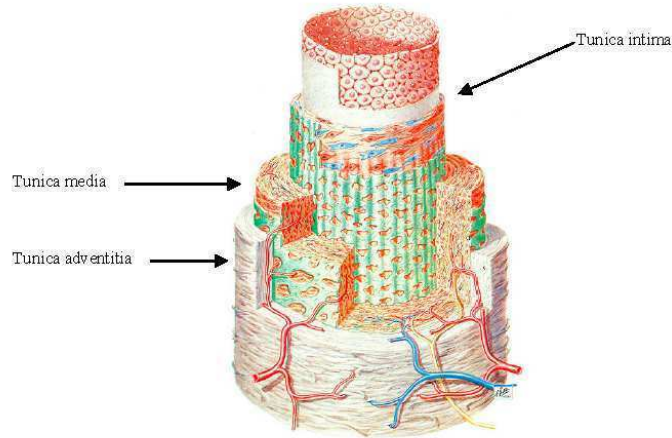


FIGURE 2: Model of the major components of a healthy artery [11]. The three main layers visible in the draw are the tunica intima, made of endothelial cells, the tunica media, made of muscle cells, elastin and collagen, and the tunica adventitia, mainly made of collagen.

by the adventitia [7].

The structure of an aneurysmatic wall can be classified accordingly to the type of tissue of the cerebral arterial wall region from which it develops. The adventitia is detected at the outer wall of aneurysms and appears stretched [8]. At the orifice of the aneurysm, the media terminates or, at most, slightly extends into the aneurysm neck region, while the elastic tissue, presumably of the IEL, may be fragmented or slightly extended [9]. Away from the orifice, the media layer is completely absent from aneurysm wall. Remnants of elastic tissue can be found at the inner wall of aneurysms [10].

Cerebral aneurysms grow over a long time scale, hence the structure of their wall undergoes to morphological changes that may differ in ruptured and unruptured aneurysms [10]. In recent hystological studies four different wall types have been detected that likely reflect consecutive stages of degeneration of aneurism wall before rupture [10].

Mechanical data for aneurysm initiation were first obtained by Scott, Ferguson, and Roach [12]. Figure 3 shows the mean stress-strain curves of cerebral arteries that underwent loading inflation and extension cyclic test. The distensibility curve abruptly changes after some runs to pressures up to 200 mmHg. These changes are not observed when the arteries are loaded to lower levels. In [12], it was conjectured that the abrupt change is related to elastin fragmentation in the arterial wall, due to mechanical loads. Notice that the curve in figure 3(b) (after change), returns to a relaxed state different from the undamaged one (figure 3(a)), because of a residual stress, due to the irreversible loss of elastin in

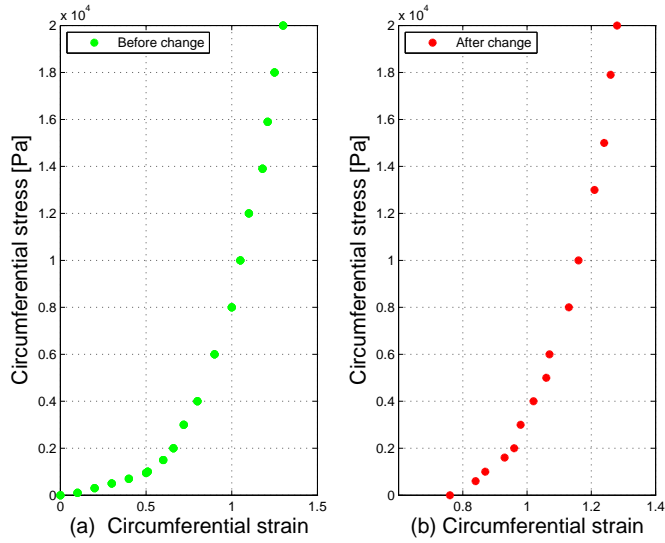


FIGURE 3: The graph shows an inflating test on a circumferential segment of sixteen anterior carotid arteries. Figure (a) represents the mechanical response of the arterial wall during some initial runs, up to a pressure of 200 mmHg. After some runs an abrupt change in the arterial wall occurs and its new mechanical behavior is represented by Figure (b) (Data from [12]).

the arterial wall.

1.2 Classification and treatment of cerebral aneurysms

There are three types of cerebral aneurysms. A saccular aneurysm is a rounded or pouch-like sac that is attached by a well-defined neck to an artery or a branch of a blood vessel. Also known as a *berry aneurysm* (because it resembles a berry hanging from a vine), this most common form of cerebral aneurysm is typically found on arteries at the base of the brain. Saccular aneurysms most often occur in adults. A lateral aneurysm appears as a bulge in the wall of the blood vessel, while a fusiform aneurysm is formed by the widening along the wall of the vessel. Aneurysms are also classified by size. Small aneurysms are less than 11 millimeters in diameter, large aneurysms are 11-25 millimeters, and giant aneurysms are greater than 25 millimeters in diameter [13].

The causes of cerebral aneurysms formation are a subject of intense investigation. In some specific cases inherited and acquired risk factors have been related to their pathologic onset [14]. Mainly hereditary connective tissue disorders have been associated with aneurysm formation, presumably as a result of the weakening of the vascular wall. Some other diseases show connection with cerebral aneurysms, as coarctation of the aorta artery or fibromuscular dysplasia, most likely because of the elevated blood pressure that occurs in these conditions.

Moreover a connection between brain aneurysms and cocaine use or general drugs abuse has been noted. This association is thought to be due to increased turbulence of blood flow and repeated, transient cases of hypertension [14]. However, the causes of initiation, development and rupture of most aneurysms is still not known.

There are many imaging techniques for intracranial aneurysms identification, such as the intra-arterial digital subtraction angiography, magnetic resonance angiography, computed tomographic angiography, and transcranial Doppler ultrasonography. Some of these medical practices are invasive because they are carried out by means of X-ray techniques and other are expensive, so that they are not used for screening [1]. This is the main reason there is much more information on ruptured aneurysms rather than unruptured ones. One of the main studies on unruptured aneurysm is the *ISUIA* (International Study of Unruptured Intracranial Aneurysms), evaluating the risk of aneurysms rupture throughout clinical examinations of approximate 2000 patient records dating back to 1998 [15]. Often unruptured aneurysms are discovered accidentally and in these cases it is not well understood which is the right strategy. When the aneurysm is big, it is usually treated, when the size is small, there is no general indication about the treatment to employ. Many small aneurysms never rupture [1], but there is no rule.

Nowadays there are few techniques to treat unruptured aneurysms. The most invasive one is the clipping technique, that implies an open brain surgery to insert a clip that closes the aneurysm neck [16]. Less invasive is the coiling technique, that consists of inserting a coil by means of an endoscopic procedure. The coil fills the bleb and causes a cloth formation inside the aneurysm [17]. More recently, the adoption of vascular endoprotheses (“flow diverting” stents) together with coiling, is increasing, with the aim of protecting the aneurysm sac from the blood flow. All these techniques are well known. However they may cause complications, so it is extremely important to have some auxiliary treatment tools and also have more information about the aneurysm pathology to help in the selection of a treatment strategy [18] [19].

2 Multi-mechanism model

In this section the basic kinematics, the stress and elasticity tensors for a multi-mechanism model are presented. Focusing on the specific application of arterial wall, we consider two strain energy functions: one of the elastin component of arterial wall and the other related to collagen fibers. Restricting attention to an homogeneous hyperelastic material, the combination of the two mechanisms can suitably represent the non-linear and inelastic behavior of arterial wall. At low level of deformations, only elastin contributes to tension, while for larger deformations, the collagen starts to bear load. Hence the two mechanisms are triggered in different ranges of deformation.

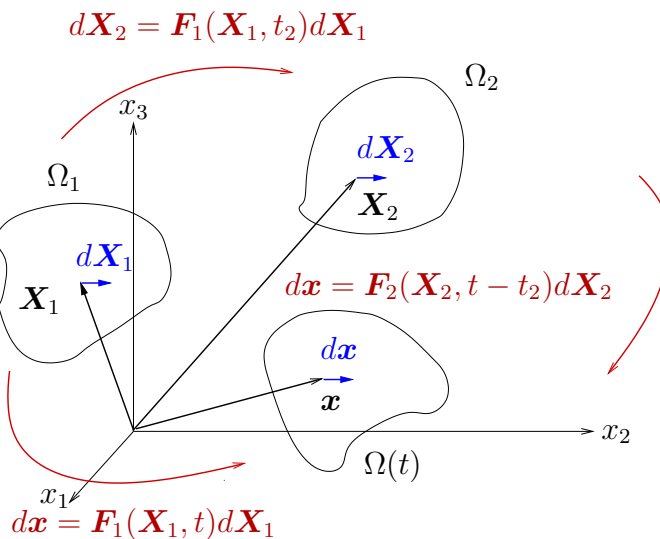


FIGURE 4: The two reference configuration of the model: Ω_1 is related to the elastin mechanism and Ω_2 to the collagen mechanism. $\Omega(t)$ is the current configuration.

2.1 Kinematics of a multi-mechanism model

Let us consider a body \mathcal{B} and a bounded domain $\Omega_1 \subseteq \mathbb{R}^3$ which represents the region occupied by the body in its reference, stress free, configuration. Associated with Ω_1 there is a time reference frame, so that the body is in reference configuration Ω_1 at time $t = t_1$. At this stage the position of a material point $P_1 \in \Omega_1$ is identified by the vector \mathbf{X}_1 as shown in figure 4.

During the motion, the body \mathcal{B} leaves its undeformed state to reach a current configuration $\Omega(t)$, $t > t_1$, where the position vector of a material point is $\mathbf{x} = \chi_1(\mathbf{X}_1, t)$. The vector function $\chi_1(\mathbf{X}_1, t)$ is a smooth, single-valued function, invertible and continuously differentiable with respect to its arguments as many times as required. The deformation gradient related to this motion is:

$$\mathbf{F}_1(\mathbf{X}_1, t) = \frac{\partial \chi_1(\mathbf{X}_1, t)}{\partial \mathbf{X}_1}, \quad (1)$$

where the subscript “1” denotes all the quantities evaluated in the reference configuration Ω_1 .

During this first stage of the deformation, only elastin contributes to the mechanical behavior of the body, so that the stress tensor depends only on $\mathbf{F}_1(\mathbf{X}_1, t)$, like a standard single mechanism elastic material.

The strain energy function per unit volume, in the reference configuration Ω_1 , is

$$W(t) = W_1(\mathbf{F}_1(\mathbf{X}_1, t)). \quad (2)$$

When the body reaches configuration $\Omega_2 = \Omega(t_2)$ the recruitment of collagen fibers occurs. As the body deforms further, corresponding to increased values of deformation, both mechanisms are active and contribute the load bearing. Adopting now Ω_2 as a reference configuration for the second mechanism, a material point position, in such a reference configuration, is identified by the position vector:

$$\mathbf{X}_2 = \mathbf{x}(\mathbf{X}_1, t_2) = \boldsymbol{\chi}_1(\mathbf{X}_1, t_2), \quad (3)$$

and, in the current configuration $\Omega(t)$, $t > t_2$, the position of a material particle can be represented by the position vector:

$$\mathbf{x} = \boldsymbol{\chi}_2(\mathbf{X}_2, t - t_2), \quad (4)$$

where the vector function $\boldsymbol{\chi}_2(\mathbf{X}_2, t - t_2)$ as well, is a smooth, single-valued function, invertible and continuously differentiable with respect to its arguments many times as required. If we define a new reference time frame t' in Ω_2 such that $t' = t - t_2$, (4) becomes $\mathbf{x} = \boldsymbol{\chi}_2(\mathbf{X}_2, t')$, and the deformation gradient that describes the motion from the reference configuration Ω_2 is:

$$\mathbf{F}_2(\mathbf{X}_2, t') = \frac{\partial \mathbf{x}(\mathbf{X}_2, t')}{\partial \mathbf{X}_2} = \frac{\partial \boldsymbol{\chi}_2(\mathbf{X}_2, t')}{\partial \mathbf{X}_2}, \quad (5)$$

where now the subscript index "2" denotes that all the variables are referred to Ω_2 .

In the current configuration $\Omega(t)$ an infinitesimal displacement $d\mathbf{x}$ can be related to both reference configurations as follows

$$d\mathbf{x} = \mathbf{F}_1(\mathbf{X}_1, t)d\mathbf{X}_1 = \mathbf{F}_2(\mathbf{X}_2, t')d\mathbf{X}_2. \quad (6)$$

By means of (6) and (3) we can find the relation between the deformation gradients

$$\mathbf{F}_2(\mathbf{X}_2, t') = \mathbf{F}_1(\mathbf{X}_1, t) \mathbf{F}_1^{-1}(\mathbf{X}_1, t_2), \quad (7)$$

where the tensor $\mathbf{F}_1^{-1}(\mathbf{X}_1, t_2)$ is known. We can now compute the determinant of each term of equation (7) as

$$\det(\mathbf{F}_2(\mathbf{X}_2, t')) = \det(\mathbf{F}_1(\mathbf{X}_1, t)) \det(\mathbf{F}_1^{-1}(\mathbf{X}_1, t_2)). \quad (8)$$

If we denote $J_2(t') = \det(\mathbf{F}_2(\mathbf{X}_2, t'))$ and $J_1(t) = \det(\mathbf{F}_1(\mathbf{X}_1, t))$, we have the relation

$$J_2(t') = J_1(t) (J_1(t_2))^{-1}, \quad (9)$$

where $(J_1(t_2))^{-1}$ is related to the reference configuration Ω_2 and it is a known scalar value constant in time, after the collagen recruitment has occurred.

The infinitesimal volume transformation among all configurations is

$$d\Omega(t) = J_1(t)d\Omega_1 = J_2(t')d\Omega_2, \quad (10)$$

so that the relation between an infinitesimal volume element in Ω_1 and Ω_2 reads

$$d\Omega_2 = J_1(t)(J_2(t'))^{-1}d\Omega_1, \quad (11)$$

and from (9) we finally have

$$d\Omega_2 = J_1(t_2)d\Omega_1. \quad (12)$$

After collagen recruitment, the strain energy function associated with the hyperelastic material has contribution from both mechanisms

$$W(t) = W_{1,2}(\mathbf{F}_1(\mathbf{X}_1, t), \mathbf{F}_2(\mathbf{X}_2, t')). \quad (13)$$

When a second critical value of deformation is reached, we hypothesize that elastin starts to degrade, and the first mechanism is weakened.

Before elastin breakage happens, the material behavior is purely elastic, i.e. after unloading it is able to recover the initial configuration Ω_1 . Due to the irreversible nature of elastin breakage, in the unloading stage, the material is no longer able to recover the configuration Ω_1 , but it eventually reaches another reference configuration $\hat{\Omega}$ that depends on the entity of the elastin damage. In particular, when all the elastin is broken, $\hat{\Omega}$ corresponds to Ω_2 , only due to relaxed collagen fibers.

W_1 and W_2 have to be invariant with respect to superimposed rigid rotations relative to the correspondent reference configuration Ω_1 and Ω_2 . The most general strain energy functions satisfying the invariance requirements are expressed by

$$W_1 = \tilde{W}_1(\mathbf{C}_1), \quad \text{and} \quad W_2 = \tilde{W}_2(\mathbf{C}_2), \quad (14)$$

where \mathbf{C}_1 and \mathbf{C}_2 are the right Cauchy-Green tensors of the first and second mechanism, respectively

$$\mathbf{C}_1 = \mathbf{F}_1^T \mathbf{F}_1, \quad \text{and} \quad \mathbf{C}_2 = \mathbf{F}_2^T \mathbf{F}_2. \quad (15)$$

With a further hypothesis of isotropy (which is definitely acceptable for elastin mechanism), without loss in generality, the strain energy functions take the form

$$W_1 = \check{W}_1(I_1, II_1, III_1), \quad \text{and} \quad W_2 = \check{W}_2(I_2, II_2, III_2), \quad (16)$$

where (I_1, II_1, III_1) and (I_2, II_2, III_2) are the principal invariants of \mathbf{C}_1 and \mathbf{C}_2 respectively. Collagen fibers are instead arranged with a specific orientation through the arterial wall and we should introduce in W_2 a dependence to account for the anisotropy of fibers, as explained in [20]. As the focus of this work is the implementation of the multi-mechanism model, at the moment we accept the isotropy hypothesis for collagen too, with future expectative of correcting it.

The last assumption is that the two mechanisms are independent, so that the strain energy function when both elastin and collagen are active is

$$W_{1,2} = W_1 + W_2. \quad (17)$$

The two mechanisms represent the independent behavior of elastin and collagen, respectively. This assumption is largely supported by the fact that both materials are found in distinct layers in the arterial wall [21].

2.2 Strain energy function

Let us observe that W_1 and W_2 are strain energy functions per unit volume defined in the reference configuration Ω_1 and Ω_2 , respectively. In order to have a complete description in terms of energy of the multi-mechanism model, we need to refer both the energies to only one reference configuration.

As first step, let us observe that the conservation of mass holds:

$$\int_{\Omega(t)} \rho \, d\Omega = \int_{\Omega_1} \rho_1 \, d\Omega_1 = \int_{\Omega_2} \rho_2 \, d\Omega_2, \quad (18)$$

where ρ is the mass density represented in the current configuration and ρ_1 and ρ_2 are respectively the mass densities in Ω_1 and Ω_2 . If we choose as unique reference configuration Ω_1 , by employing (12) and (10), the previous integrals rewrite

$$\int_{\Omega_1} \rho J_1(t) \, d\Omega_1 = \int_{\Omega_1} \rho_1 \, d\Omega_1 = \int_{\Omega_1} \rho_2 J_1(t_2) \, d\Omega_1, \quad (19)$$

where

$$\rho_2 = \rho_1 J_1(t_2)^{-1} \quad \text{and} \quad \rho = \rho_1 J_1(t)^{-1} \quad (20)$$

are two relations that allow to relate the mass density in $\Omega(t)$ and Ω_2 with the mass density in Ω_1 . By means of (10), the total energy in the current configuration $\Omega(t)$, when both mechanisms are active, is expressed by

$$\mathcal{U}_{tot} = \int_{\Omega(t)} J_1^{-1}(t) W_1 \, d\Omega + \int_{\Omega(t)} J_2^{-1}(t') W_2 \, d\Omega, \quad (21)$$

such that

$$\mathcal{U}_1 = \int_{\Omega(t)} J_1^{-1}(t) W_1 \, d\Omega, \quad \text{and} \quad \mathcal{U}_2 = \int_{\Omega(t)} J_2^{-1}(t') W_2 \, d\Omega, \quad (22)$$

where \mathcal{U}_1 is the energy associated to the first mechanism and \mathcal{U}_2 to the second. If we express the total energy with respect to the reference configuration Ω_1 , from equation (21), by means of the relation (12), we have

$$\mathcal{U}_{tot} = \int_{\Omega_1} W_1 \, d\Omega_1 + \int_{\Omega_1} J_2^{-1}(t') J_1(t) W_2 \, d\Omega_1. \quad (23)$$

The insertion of relation (9) in the previous one gives

$$\mathcal{U}_{tot} = \int_{\Omega_1} W_1 \, d\Omega_1 + \int_{\Omega_1} J_1(t_2) W_2 \, d\Omega_1, \quad (24)$$

where we recall that $J_1(t_2)$ is known after the collagen recruitment has occurred. If we define W_{tot} as the total strain energy per unit volume in Ω_1 , such that

$$\mathcal{U}_{tot} = \int_{\Omega_1} W_{tot} \, d\Omega_1, \quad (25)$$

because all the integrals are referred to the volume occupied by the body in the reference configuration Ω_1 , when both mechanisms are active, we have

$$W_{tot} = W_1 + J_1(t_2) W_2. \quad (26)$$

2.3 Stress and elasticity tensors

In this paragraph we introduce the *multiplicative decomposition* of the deformation gradient \mathbf{F} into an *isochoric* (or *distortional*) and a *volumetric* (or *dilational*) part [22] [23] [11], to derive the stress tensors for a weakly compressible material.

The multiplicative decomposition of the deformation gradient \mathbf{F} reads

$$\mathbf{F} = \hat{\mathbf{F}}\bar{\mathbf{F}}, \quad (27)$$

where $\bar{\mathbf{F}} = J^{-\frac{1}{3}}\mathbf{F}$ is the isochoric part, and $\hat{\mathbf{F}} = J^{\frac{1}{3}}\mathbf{I}$ is the volumetric part, with \mathbf{I} the second order identity tensor. The isochoric part of the deformation gradient takes into account the deformation without change in volume, so that $\det \bar{\mathbf{F}} = 1$. The volumetric part contains all the volumetric deformation contributions, and $\det \hat{\mathbf{F}} = J$.

In the same way, we can derive the multiplicative decomposition of the right and left Cauchy-Green tensors:

$$\mathbf{C} = \mathbf{F}^T\mathbf{F} = (\hat{\mathbf{F}}\bar{\mathbf{F}})^T\hat{\mathbf{F}}\bar{\mathbf{F}} = (\bar{\mathbf{F}})^T(\hat{\mathbf{F}})^T\hat{\mathbf{F}}\bar{\mathbf{F}} = J^{\frac{2}{3}}(\bar{\mathbf{F}})^T\bar{\mathbf{F}}, \quad (28)$$

$$\mathbf{B} = \mathbf{F}\mathbf{F}^T = \hat{\mathbf{F}}\bar{\mathbf{F}}(\hat{\mathbf{F}}\bar{\mathbf{F}})^T = \bar{\mathbf{F}}\hat{\mathbf{F}}(\hat{\mathbf{F}})^T(\bar{\mathbf{F}})^T = J^{\frac{2}{3}}\bar{\mathbf{F}}(\bar{\mathbf{F}})^T, \quad (29)$$

and define the *unimodular right* and *left* Cauchy-Green tensors as the isochoric part of \mathbf{C} and \mathbf{B} :

$$\bar{\mathbf{C}} = \bar{\mathbf{F}}^T\bar{\mathbf{F}} = J^{-\frac{2}{3}}\mathbf{C}, \quad \text{with} \quad \det \bar{\mathbf{C}} = 1, \quad (30)$$

$$\bar{\mathbf{B}} = \bar{\mathbf{F}}\bar{\mathbf{F}}^T = J^{-\frac{2}{3}}\mathbf{B}, \quad \text{with} \quad \det \bar{\mathbf{B}} = 1. \quad (31)$$

In particular, together with the invariants of \mathbf{C} we introduce the modified invariants of $\bar{\mathbf{C}}$ as

$$I_C = \text{tr}\mathbf{C}, \quad II_C = \frac{1}{2}((\text{tr}\mathbf{C})^2 - \text{tr}(\mathbf{C}^2)), \quad III_C = \det \mathbf{C} = J^2, \quad (32)$$

$$I_{\bar{\mathbf{C}}} = \text{tr}\bar{\mathbf{C}}, \quad II_{\bar{\mathbf{C}}} = \frac{1}{2}((\text{tr}\bar{\mathbf{C}})^2 - \text{tr}(\bar{\mathbf{C}}^2)), \quad III_{\bar{\mathbf{C}}} = 1, \quad (33)$$

and similar definitions hold for \mathbf{B} and $\bar{\mathbf{B}}$.

The use of (27), supplies the correspondent strain energy function for an isotropic frame indifferent material [23] splitted as

$$W(J, I_{\bar{\mathbf{C}}}, II_{\bar{\mathbf{C}}}) = W_{vol}(J) + W_{iso}(I_{\bar{\mathbf{C}}}, II_{\bar{\mathbf{C}}}), \quad (34)$$

where:

- 1) W_{vol} depends merely on the volume changing part throughout J .
- 2) W_{iso} is purely isochoric and depends on the invariants of the unimodular right Cauchy-Green $\bar{\mathbf{C}}$.

Let us derive now the stress tensors for a weakly compressible material. The use of the decomposition technique (34) allows us to express componentwise the second Piola-Kirchhoff stress tensor \mathbf{S} as

$$S_{AB} = 2 \frac{dW}{dC_{AB}} = 2 \left(\frac{dW_{vol}}{dC_{AB}} + \frac{dW_{iso}}{dC_{AB}} \right), \quad (35)$$

where the volumetric contribution is

$$\begin{aligned} \frac{dW_{vol}}{dC_{AB}} &= \frac{dW_{vol}}{dJ} \frac{dJ}{dC_{AB}} = W'_{vol} \frac{d(\sqrt{\det \mathbf{C}})}{dC_{AB}} = \\ &= W'_{vol} \frac{1}{2\sqrt{\det \mathbf{C}}} \frac{d(\det \mathbf{C})}{dC_{AB}} = W'_{vol} \frac{1}{2\sqrt{\det \mathbf{C}}} (\det \mathbf{C}) C_{AB}^{-1} = \\ &= \frac{1}{2} W'_{vol} \sqrt{\det \mathbf{C}} C_{AB}^{-1} = \frac{1}{2} W'_{vol} J C_{AB}^{-1}, \end{aligned} \quad (36)$$

and the isochoric part is

$$\frac{dW_{iso}}{dC_{AB}} = \frac{dW_{iso}}{d\bar{\mathbf{C}}_{MN}} \frac{d\bar{\mathbf{C}}_{MN}}{dC_{AB}}. \quad (37)$$

Let us compute each term of (37) separately:

$$\begin{aligned} \frac{dW_{iso}}{d\bar{\mathbf{C}}_{MN}} &= \frac{\partial W_{iso}}{\partial I_{\bar{\mathbf{C}}}} \frac{\partial I_{\bar{\mathbf{C}}}}{\partial \bar{\mathbf{C}}_{MN}} + \frac{\partial W_{iso}}{\partial II_{\bar{\mathbf{C}}}} \frac{\partial II_{\bar{\mathbf{C}}}}{\partial \bar{\mathbf{C}}_{MN}} \\ &= \frac{\partial W_{iso}}{\partial I_{\bar{\mathbf{C}}}} \delta_{MN} + \frac{\partial W_{iso}}{\partial II_{\bar{\mathbf{C}}}} (I_{\bar{\mathbf{C}}} \delta_{MN} - \bar{\mathbf{C}}_{MN}), \end{aligned} \quad (38)$$

and

$$\begin{aligned} \frac{d\bar{\mathbf{C}}_{MN}}{dC_{AB}} &= \frac{d(J^{-2/3} C_{MN})}{dC_{AB}} = \frac{d((\det \mathbf{C})^{-1/3} C_{MN})}{dC_{AB}} \\ &= -\frac{1}{3} (\det \mathbf{C})^{-4/3} \frac{d(\det \mathbf{C})}{dC_{AB}} C_{MN} + (\det \mathbf{C})^{-1/3} \frac{dC_{MN}}{dC_{AB}} \\ &= -\frac{1}{3} (\det \mathbf{C})^{-1/3} C_{AB}^{-1} C_{MN} + (\det \mathbf{C})^{-1/3} \delta_{AM} \delta_{BN} = \\ &= J^{-2/3} (\delta_{AM} \delta_{BN} - \frac{1}{3} C_{AB}^{-1} C_{MN}). \end{aligned} \quad (39)$$

If we define the fourth order tensor $\mathbb{P}_{ABMN} = (\delta_{AM} \delta_{BN} - \frac{1}{3} C_{AB}^{-1} C_{MN})$, finally the second Piola-Kirchhoff stress tensor reads

$$S_{AB} = W'_{vol} J C_{AB}^{-1} + 2J^{-2/3} (\mathbb{P}_{ABMN}) \left(\frac{\partial W_{iso}}{\partial I_{\bar{\mathbf{C}}}} \delta_{MN} + \frac{\partial W_{iso}}{\partial II_{\bar{\mathbf{C}}}} (I_{\bar{\mathbf{C}}} \delta_{MN} - \bar{\mathbf{C}}_{MN}) \right), \quad (40)$$

where the stress is composed by

$$(S_{vol})_{AB} = W'_{vol} J C_{AB}^{-1}, \quad (41)$$

$$(S_{iso})_{AB} = 2J^{-2/3} (\mathbb{P}_{ABMN}) \left(\frac{\partial W_{iso}}{\partial I_{\bar{\mathbf{C}}}} \delta_{MN} + \frac{\partial W_{iso}}{\partial II_{\bar{\mathbf{C}}}} (I_{\bar{\mathbf{C}}} \delta_{MN} - \bar{\mathbf{C}}_{MN}) \right). \quad (42)$$

From equation (35) and the definition of the first Piola-Kirchhoff stress tensor \mathbf{P} componentwise:

$$P_{iB} = F_{iA} S_{AB}, \quad (43)$$

we have

$$P_{iB} = 2F_{iA} \frac{dW}{dC_{AB}} = 2F_{iA} \left(\frac{dW_{vol}}{dC_{AB}} + \frac{dW_{iso}}{dC_{AB}} \right). \quad (44)$$

With similar calculation as before the volumetric and isochoric parts of the stress tensor read

$$(P_{vol})_{iB} = JW'_{vol} F_{iB}^{-T}, \quad (45)$$

$$(P_{iso})_{iB} = 2J^{-2/3} F_{iA} (\mathbb{P}_{ABMN}) \left(\frac{\partial W_{iso}}{\partial I_{\bar{C}}} \delta_{MN} + \frac{\partial W_{iso}}{\partial II_{\bar{C}}} (I_{\bar{C}} \delta_{MN} - \bar{C}_{MN}) \right) \quad (46)$$

We can now evaluate the Cauchy stress tensor \mathbf{T} in the current configuration; componentwise

$$T_{ij} = J^{-1} F_{iA} S_{AB} F_{jB}, \quad (47)$$

hence from (35)

$$T_{ij} = 2J^{-1} F_{iA} \frac{dW}{dC_{AB}} F_{jB} = 2J^{-1} F_{iA} \left(\frac{dW_{vol}}{dC_{AB}} + \frac{dW_{iso}}{dC_{AB}} \right) F_{jB}, \quad (48)$$

and the Cauchy stress tensor decomposes as

$$(T_{vol})_{ij} = W'_{vol} \delta_{ij}, \quad (49)$$

$$(T_{iso})_{ij} = 2J^{-5/3} F_{iA} (\mathbb{P}_{ABMN}) \left(\frac{\partial W_{iso}}{\partial I_{\bar{C}}} \delta_{MN} + \frac{\partial W_{iso}}{\partial II_{\bar{C}}} (I_{\bar{C}} \delta_{MN} - \bar{C}_{MN}) \right) F_{jB} \quad (50)$$

We observe that, by construction, in the current configuration the volumetric part of the stress tensor is spherical, as the hydrostatic pressure in incompressible materials.

In the balance of linear momentum we employ the first Piola-Kirchhoff stress tensor \mathbf{P} , hence in the following all the calculation are made in terms of \mathbf{P} .

Finally, we introduce the fourth order elasticity tensors, obtained by:

$$\mathbb{C}_{vol} = \frac{\partial \mathbf{P}_{vol}}{\partial \mathbf{F}}, \quad \text{and} \quad \mathbb{C}_{iso} = \frac{\partial \mathbf{P}_{iso}}{\partial \mathbf{F}}. \quad (51)$$

2.4 Collagen recruitment

The collagen recruitment and the elastin breakage are introduced on the basis of an invariant scalar function s that measures the deformation [24]:

$$s(\bar{\mathbf{C}}_1) = \hat{s}(\bar{\mathbf{C}}_1(\mathbf{X}_1, t), \mathbf{x}). \quad (52)$$

If the measure is homogeneous, there is no direct dependence on the position \mathbf{x} . During the motion, the collagen activation occurs at a threshold value $s = s_a$,

and at the corresponding material point, all the collagen fibers are recruited simultaneously. If the deformation is non-uniform, the activation criterion can be satisfied at different times in different points of the body; moreover for an inhomogeneous body, s_a will depend on the material position too.

For isotropic materials, we may express the homogeneous measure s as:

$$s(\bar{\mathbf{C}}_1) = \frac{1}{C_s} W_{1iso}(I_{\bar{\mathbf{C}}_1}, II_{\bar{\mathbf{C}}_1}), \quad (53)$$

where C_s is a convenient coefficient with dimension of Pa^{-1} and W_{1iso} is the isochoric strain energy function of the first mechanism.

Finally, by means of the total strain energy function (26), we can express the contribution of both mechanisms in the reference configuration Ω_1 as

$$W_{tot} = \begin{cases} W_1 & \text{for } 0 \leq s \leq s_a, \\ W_1 + J_1(t_2)W_2 & \text{for } s > s_a. \end{cases} \quad (54)$$

The use of equation (34) for a multi-mechanism model leads to split further the energy into W_{1vol} and W_{2vol} , representing the change in volume of the body during the motion, while W_{1iso} and W_{2iso} represent the incompressible contributions of each mechanism. Hence (54) becomes

$$W_{tot} = \begin{cases} W_{1vol} + W_{1iso} & \text{for } 0 \leq s \leq s_a, \\ W_{1vol} + W_{1iso} + J_1(t_2)(W_{2vol} + W_{2iso}) & \text{for } s > s_a. \end{cases} \quad (55)$$

To write the balance of linear momentum in the reference configuration Ω_1 we need to derive the first Piola-Kirchhoff stress tensor of a multi-mechanism. In the following we explicitly indicate the dependence on different time frames when needed for clarity:

$$\mathbf{P}_1(t) = \mathbf{P}(t)_{1vol} + \mathbf{P}(t)_{1iso}, \quad \text{and} \quad \mathbf{P}_2(t') = \mathbf{P}(t')_{2vol} + \mathbf{P}(t')_{2iso}, \quad (56)$$

that, by means of (45) and (46), may be rewritten as:

$$\mathbf{P}(t)_{1vol} = J_1(t) \frac{dW_{1vol}}{dJ_1(t)} \mathbf{F}_1(t)^{-T}, \quad (57)$$

$$\mathbf{P}(t)_{1iso} = 2J_1(t)^{-2/3} \mathbf{F}_1(t) \mathbb{P}_1 : \left(\frac{dW_{1iso}}{d\bar{\mathbf{C}}_1} \right), \quad (58)$$

and

$$\mathbf{P}(t')_{2vol} = J_2(t') \frac{dW_{2vol}}{dJ_2(t')} \mathbf{F}_2(t')^{-T}, \quad (59)$$

$$\mathbf{P}(t')_{2iso} = 2J_2(t')^{-2/3} \mathbf{F}_2(t') \mathbb{P}_2 : \left(\frac{dW_{2iso}}{d\bar{\mathbf{C}}_2} \right). \quad (60)$$

To simplify the notation, let us define

$$\mathbf{F}_1(\mathbf{X}_1, t_2) = \mathbf{F}^* \quad \text{and} \quad J_1(t_2) = J^*. \quad (61)$$

hence from (7) and (9), we have

$$\mathbf{F}_2(t') = \mathbf{F}_1(t)(\mathbf{F}^*)^{-1} \quad \text{and} \quad J_2(t') = J_1(t)(J^*)^{-1}. \quad (62)$$

The replacement of (62) in (59) and (60) allows us to pull back the first Piola-Kirchhoff of the second mechanism \mathbf{P}_2 to the reference configuration Ω_1 .

When $\mathbf{P}(t)_{2\,vol}$ and $\mathbf{P}(t)_{2\,iso}$ are expressed with respect to the first reference configuration Ω_1 , we may neglect in notation their dependence over time, and the total first Piola-Kirchhoff stress tensor for a multi-mechanism model reads

$$\mathbf{P} = \begin{cases} \mathbf{P}_{1\,vol} + \mathbf{P}_{1\,iso} & \text{for } 0 \leq s \leq s_a, \\ \mathbf{P}_{1\,vol} + \mathbf{P}_{1\,iso} + J^*(\mathbf{P}_{2\,vol} + \mathbf{P}_{2\,iso}) & \text{for } s > s_a. \end{cases} \quad (63)$$

The stress tensors \mathbf{P}_1 and \mathbf{P}_2 are strongly non-linear, hence to linearize and solve the balance of linear momentum, we need to compute the fourth order elasticity tensors. By means of (51) we find

$$\mathbb{C}_1 = \frac{\partial \mathbf{P}_1}{\partial \mathbf{F}_1}, \quad \text{and} \quad \mathbb{C}_2 = \frac{\partial \mathbf{P}_2}{\partial \mathbf{F}_1}, \quad (64)$$

where both \mathbb{C}_1 and \mathbb{C}_2 are obtained deriving \mathbf{P}_1 and \mathbf{P}_2 with respect to \mathbf{F}_1 , because both of them refer to the first reference configuration Ω_1 .

We observe that in Finite Element Method procedure, the linearization of the stress tensors \mathbf{P}_1 and \mathbf{P}_2 is obtained by computing their *Frechet* derivative in the direction of an increment $\delta \mathbf{F}_1$ of the deformation gradient. We indicate these derivatives as:

$$\mathcal{D}_{F_1} \mathbf{P}_1[\delta \mathbf{F}_1] = \frac{\partial \mathbf{P}_1}{\partial \mathbf{F}_1} : \delta \mathbf{F}_1, \quad \text{and} \quad \mathcal{D}_{F_1} \mathbf{P}_2[\delta \mathbf{F}_1] = \frac{\partial \mathbf{P}_2}{\partial \mathbf{F}_1} : \delta \mathbf{F}_1, \quad (65)$$

where “:” denotes the tensor operation obtained by saturation of the last two indices of the tensors involved, and the result is a second order tensor. Thanks to definition (64) we have:

$$\mathcal{D}_{F_1} \mathbf{P}_1[\delta \mathbf{F}_1] = \mathbb{C}_1 : \delta \mathbf{F}_1, \quad \text{and} \quad \mathcal{D}_{F_1} \mathbf{P}_2[\delta \mathbf{F}_1] = \mathbb{C}_2 : \delta \mathbf{F}_1, \quad (66)$$

that represent the linearization of stress tensors \mathbf{P}_1 and \mathbf{P}_2 with respect of an increment of deformation $\delta \mathbf{F}_1$.

2.4.1 Volumetric stress and elasticity tensors

To compute the volumetric part of the stress tensor for the first and second mechanism, we introduce the volumetric strain energy function per unit volume:

$$W_{i\,vol} = \frac{K_i}{4}((J_i - 1)^2 + (\ln J_i)^2), \quad \text{with } i = 1, 2, \quad (67)$$

where K_i is the *compression modulus* (or *bulk modulus*), and expression (67) holds for both elastin and collagen (respectively $i = 1, 2$).

The derivative of W_{ivol} with respect to J_i reads

$$\frac{dW_{ivol}}{dJ_i} = \frac{K_i}{2}(J_i - 1 + \frac{1}{J_i}\ln J_i), \quad \text{with } i = 1, 2. \quad (68)$$

From (57), the volumetric part of the first Piola-Kirchhoff stress tensor for the first mechanism is:

$$\mathbf{P}_{1vol} = \frac{K_1}{2}J_1(J_1 - 1 + \frac{1}{J_1}\ln J_1)\mathbf{F}_1^{-T} = \frac{K_1}{2}(J_1^2 - J_1 + \ln J_1)\mathbf{F}_1^{-T}, \quad (69)$$

and, from (59), the stress tensor for the second mechanism is

$$\mathbf{P}_{2vol} = \frac{K_2}{2}J_2(J_2 - 1 + \frac{1}{J_2}\ln J_2)\mathbf{F}_2^{-T}. \quad (70)$$

We need to replace expression (62) in (70) to pull back \mathbf{P}_{2vol} to Ω_1 :

$$\begin{aligned} \mathbf{P}_{2vol} &= \frac{K_2}{2} \frac{J_1}{J^*} \left(\frac{J_1}{J^*} - 1 + \frac{J^*}{J_1} \ln \left(\frac{J_1}{J^*} \right) \right) (\mathbf{F}_1 (\mathbf{F}^*)^{-1})^{-T} \\ &= \frac{K_2}{2} \left(\left(\frac{J_1}{J^*} \right)^2 - \frac{J_1}{J^*} + \ln \left(\frac{J_1}{J^*} \right) \right) \mathbf{F}_1^{-T} (\mathbf{F}^*)^T \end{aligned} \quad (71)$$

The volumetric part of the stress tensor, obtained by adding (69) and (71) is non-linear with respect to the deformation gradient \mathbf{F}_1 .

The fourth order elasticity tensors are:

$$\mathbb{C}_{1vol} = \frac{\partial \mathbf{P}_{1vol}}{\partial \mathbf{F}_1}, \quad \text{and} \quad \mathbb{C}_{2vol} = \frac{\partial \mathbf{P}_{2vol}}{\partial \mathbf{F}_1}. \quad (72)$$

From (65, 72) the linearization of \mathbf{P}_{1vol} reads:

$$\begin{aligned} \mathbb{C}_{1vol} : \delta \mathbf{F}_1 &= \frac{K_1}{2} J_1 \left(2J_1 - 1 + \frac{1}{J_1} \right) (\mathbf{F}_1^{-T} : \delta \mathbf{F}_1) \mathbf{F}_1^{-T} \\ &\quad - \frac{K_1}{2} (J_1^2 - J_1 + \ln J_1) \mathbf{F}_1^{-T} \delta \mathbf{F}_1^T \mathbf{F}_1^{-T}, \end{aligned} \quad (73)$$

and the linearization of \mathbf{P}_{2vol} is:

$$\begin{aligned} \mathbb{C}_{2vol} : \delta \mathbf{F}_1 &= \frac{K_2}{2} J_1 \left(2 \frac{J_1}{J^{*2}} - \frac{1}{J^*} + 1 \right) (\mathbf{F}_1^{-T} : \delta \mathbf{F}_1) \mathbf{F}_1^{-T} \mathbf{F}^{*T} \\ &\quad - \frac{K_2}{2} \left(\left(\frac{J_1}{J^*} \right)^2 - \left(\frac{J_1}{J^*} \right) + \ln \left(\frac{J_1}{J^*} \right) \right) \mathbf{F}_1^{-T} \delta \mathbf{F}_1^T \mathbf{F}_1^{-T} \mathbf{F}^{*T}, \end{aligned} \quad (74)$$

where $\delta \mathbf{F}_1$ is a variation of \mathbf{F}_1 .

2.4.2 Isochoric stress and elasticity tensors

In this section we compute the incompressible part of the stress tensor for the multi-mechanism. To model both elastin and collagen ($k = 1, 2$) with a Neo-Hookean constitutive law we introduce the strain energy function:

$$W_{k\,iso}^{\text{NH}} = \frac{\mu_k}{2}(I_{\bar{\mathbf{C}}_k} - 3), \quad \text{with } k = 1, 2, \quad (75)$$

and

$$\frac{d(W_{k\,iso}^{\text{NH}})}{d\bar{\mathbf{C}}_k} = \frac{\partial(W_{k\,iso}^{\text{NH}})}{\partial I_{\bar{\mathbf{C}}_k}} \mathbf{I} = \frac{\mu_k}{2} \mathbf{I}, \quad \text{with } k = 1, 2, \quad (76)$$

where \mathbf{I} is the second order identity tensor.

From (58) and (76), the isochoric part of the first Piola-Kirchhoff stress tensor, for the first mechanism reads

$$\mathbf{P}_{1\,iso}^{\text{NH}} = \mu_1 J_1^{-2/3} \left(\mathbf{F}_1 - \frac{1}{3} I_{C_1} \mathbf{F}_1^{-T} \right). \quad (77)$$

To derive the isochoric part of the first Piola-Kirchhoff stress tensor, for the second mechanism, we need to compute \mathbf{C}_2 , the right Cauchy-Green tensor for the second mechanism, in terms of \mathbf{C}_1 :

$$\mathbf{C}_2 = (\mathbf{F}^*)^{-T} \mathbf{C}_1 (\mathbf{F}^*)^{-1}, \quad (78)$$

and its deviatoric part is:

$$\bar{\mathbf{C}}_2 = \left(\frac{J_1}{J^*} \right)^{-2/3} (\mathbf{F}^*)^{-T} \mathbf{C}_1 (\mathbf{F}^*)^{-1}. \quad (79)$$

Hence,

$$\begin{aligned} I_{\bar{\mathbf{C}}_2} = \text{tr} \bar{\mathbf{C}}_2 &= \left(\frac{J_1}{J^*} \right)^{-2/3} \text{tr}((\mathbf{F}^*)^{-T} \mathbf{C}_1 (\mathbf{F}^*)^{-1}) = \left(\frac{J_1}{J^*} \right)^{-2/3} \text{tr}((\mathbf{F}^*)^{-1} (\mathbf{F}^*)^{-T} \mathbf{C}_1) \\ &= \left(\frac{J_1}{J^*} \right)^{-2/3} \text{tr}((\mathbf{C}^*)^{-1} \mathbf{C}_1) = \left(\frac{J_1}{J^*} \right)^{-2/3} (\mathbf{C}^*)^{-1} : \mathbf{C}_1, \end{aligned} \quad (80)$$

where we used the relation $(\mathbf{F}^*)^T \mathbf{F}^* = \mathbf{C}^*$ and the symmetry of \mathbf{C}_1 .

Relations (60), (80) and (75), help us in deriving the expression of the isochoric part of the first Piola-Kirchhoff stress tensor, for the second mechanism

$$\mathbf{P}_{2\,iso}^{\text{NH}} = \mu_2 \left(\frac{J_1}{J^*} \right)^{-2/3} \left(\mathbf{F}_1 (\mathbf{F}^*)^{-1} - \frac{1}{3} I_{C_2} (\mathbf{F}^*)^T \mathbf{F}_1^{-T} \right). \quad (81)$$

The fourth order elasticity tensors are:

$$\mathbb{C}_{1\,iso}^{\text{NH}} = \frac{\partial \mathbf{P}_{1\,iso}^{\text{NH}}}{\partial \mathbf{F}_1}, \quad \text{and} \quad \mathbb{C}_{2\,vol}^{\text{NH}} = \frac{\partial \mathbf{P}_{2\,iso}^{\text{NH}}}{\partial \mathbf{F}_1}. \quad (82)$$

From (65, 82) the linearization of \mathbf{P}_{1iso} reads:

$$\begin{aligned}\mathbb{C}_{1iso}^{NH} : \delta \mathbf{F}_1 = & - \frac{2}{3} \mu_1 J_1^{-2/3} (\mathbf{F}_1^{-T} : \delta \mathbf{F}_1) \mathbf{F}_1 \\ & + \frac{2}{9} \mu_1 I_{\bar{\mathbf{C}}_1} (\mathbf{F}_1^{-T} : \delta \mathbf{F}_1) \mathbf{F}_1^{-T} \\ & - \frac{2}{3} \mu_1 J_1^{-2/3} (\mathbf{F}_1 : \delta \mathbf{F}_1) \mathbf{F}_1^{-T} \\ & + \mu_1 J_1^{-2/3} \delta \mathbf{F}_1 + \frac{\mu_1}{3} I_{\bar{\mathbf{C}}_1} \mathbf{F}_1^{-T} \delta \mathbf{F}_1^T \mathbf{F}_1^{-T}.\end{aligned}\quad (83)$$

and the linearization of \mathbf{P}_{2iso} is:

$$\begin{aligned}\mathbb{C}_{2iso}^{NH} : \delta \mathbf{F}_1 = & - \frac{2}{3} \mu_2 \left(\frac{J_1}{J^*} \right)^{-2/3} (\mathbf{F}_1^{-T} : \delta \mathbf{F}_1) \mathbf{F}_1 (\mathbf{F}^*)^{-1} \\ & + \frac{2}{9} \mu_2 I_{\bar{\mathbf{C}}_2} (\mathbf{F}_1^{-T} : \delta \mathbf{F}_1) (\mathbf{F}^*)^T \mathbf{F}_1^{-T} \\ & - \frac{1}{3} \mu_2 \left(\frac{J_1}{J^*} \right)^{-2/3} ((\mathbf{C}^*)^{-1} : \delta \mathbf{F}_1^T \mathbf{F}_1 + (\mathbf{C}^*)^{-1} : \mathbf{F}_1^T \delta \mathbf{F}_1) (\mathbf{F}^*)^T \mathbf{F}_1^{-T} \\ & + \mu_2 \left(\frac{J_1}{J^*} \right)^{-2/3} \delta \mathbf{F}_1 (\mathbf{F}^*)^{-1} + \frac{\mu_2}{3} I_{\bar{\mathbf{C}}_2} (\mathbf{F}^*)^T \mathbf{F}_1^{-T} \delta \mathbf{F}_1^T \mathbf{F}_1^{-T}.\end{aligned}\quad (84)$$

We observe that if $\mathbf{F}^* = \mathbf{F}_1$ then $\mathbf{P}_{2iso}^{NH} = 0$.

The other constitutive law we may use to model elastin and collagen is derived by the exponential strain energy function:

$$W_{jiso}^{Exp} = \frac{\alpha_j}{2\gamma_j} (e^{\gamma_j (I_{\bar{\mathbf{C}}_j} - 3)} - 1), \quad \text{with } j = 1, 2, \quad (85)$$

and

$$\frac{d(W_{jiso}^{Exp})}{d\bar{\mathbf{C}}_j} = \frac{\partial(W_{jiso}^{Exp})}{\partial I_{\bar{\mathbf{C}}_j}} \mathbf{I} = \frac{\alpha_j}{2} e^{\gamma_j (I_{\bar{\mathbf{C}}_j} - 3)} \mathbf{I}, \quad \text{with } j = 1, 2, \quad (86)$$

where \mathbf{I} is the second order identity tensor.

From (58) and (86), the isochoric part of the first Piola-Kirchhoff stress tensor, for the first mechanism is:

$$\mathbf{P}_{1iso}^{Exp} = \alpha_1 e^{\gamma_1 (I_{\bar{\mathbf{C}}_1} - 3)} J_1^{-2/3} \mathbf{F}_1 \left(\left(\mathbb{I} - \frac{1}{3} \mathbf{C}_1^{-1} \otimes \mathbf{C}_1 \right) : \mathbf{I} \right), \quad (87)$$

where \otimes is the outer tensor product. Finally,

$$\mathbf{P}_{1iso}^{Exp} = \alpha_1 e^{\gamma_1 (I_{\bar{\mathbf{C}}_1} - 3)} J_1^{-2/3} \left(\mathbf{F}_1 - \frac{1}{3} \mathbf{F}_1^{-T} I_{\mathbf{C}_1} \right). \quad (88)$$

From (60) and (86), the isochoric part of the stress tensor for the second mechanism is:

$$\mathbf{P}_{2iso}^{Exp} = \alpha_2 e^{\gamma_2 (I_{\bar{\mathbf{C}}_2} - 3)} \left(\frac{J_1}{J^*} \right)^{-2/3} \mathbf{F}_1 (\mathbf{F}^*)^{-1} \left(\left(\mathbb{I} - \frac{1}{3} \mathbf{C}_2^{-1} \otimes \mathbf{C}_2 \right) : \mathbf{I} \right), \quad (89)$$

where we need to introduce (78) and (80).

After some calculations

$$\mathbf{P}_{2iso}^{\text{Exp}} = \alpha_2 e^{\gamma_2(I_{\bar{C}_2}-3)} \left(\frac{J_1}{J^*}\right)^{-2/3} \left(\mathbf{F}_1(\mathbf{F}^*)^{-1} - \frac{1}{3}(\mathbf{F}^*)^T \mathbf{F}_1^{-T} I_{C_2}\right), \quad (90)$$

as in the previous case, we observe that when $\mathbf{F}^* = \mathbf{F}_1$ then $\mathbf{P}_{2iso}^{\text{Exp}} = 0$.

For the exponential material, the fourth order elasticity tensors read:

$$\mathbb{C}_{1iso}^{\text{Exp}} = \frac{\mathbf{P}_{1iso}^{\text{Exp}}}{\partial \mathbf{F}_1}, \quad \text{and} \quad \mathbb{C}_{2iso}^{\text{Exp}} = \frac{\mathbf{P}_{2iso}^{\text{Exp}}}{\partial \mathbf{F}_1}. \quad (91)$$

From (65, 91), the linearization of (88) reads:

$$\begin{aligned} \mathbb{C}_{1iso}^{\text{Exp}} : \delta \mathbf{F}_1 = & - \frac{2}{3} \alpha_1 e^{\gamma_1(I_{\bar{C}_1}-3)} J_1^{-2/3} (1 + \gamma_1 I_{\bar{C}_1}) (\mathbf{F}_1^{-T} : \delta \mathbf{F}_1) \mathbf{F}_1 \quad (92) \\ & + \frac{2}{9} \alpha_1 e^{\gamma_1(I_{\bar{C}_1}-3)} I_{\bar{C}_1} (1 + \gamma_1 I_{\bar{C}_1}) (\mathbf{F}_1^{-T} : \delta \mathbf{F}_1) \mathbf{F}_1^{-T} \\ & - \frac{2}{3} \alpha_1 e^{\gamma_1(I_{\bar{C}_1}-3)} J_1^{-2/3} (1 + \gamma_1 I_{\bar{C}_1}) (\mathbf{F}_1 : \delta \mathbf{F}_1) \mathbf{F}_1^{-T} \\ & + 2 \alpha_1 \gamma_1 e^{\gamma_1(I_{\bar{C}_1}-3)} J_1^{-4/3} (\mathbf{F}_1 : \delta \mathbf{F}_1) \mathbf{F}_1 \\ & + \alpha_1 e^{\gamma_1(I_{\bar{C}_1}-3)} J_1^{-2/3} \delta \mathbf{F}_1 \\ & + \frac{\alpha_1}{3} e^{\gamma_1(I_{\bar{C}_1}-3)} I_{\bar{C}_1} \mathbf{F}_1^{-T} \delta \mathbf{F}_1^T \mathbf{F}_1^{-T}. \end{aligned}$$

and the linearization of (90) results:

$$\begin{aligned} \mathbb{C}_{2iso}^{\text{Exp}} : \delta \mathbf{F}_1 = & - \frac{2}{3} \alpha_2 e^{\gamma_2(I_{\bar{C}_2}-3)} \left(\frac{J_1}{J^*}\right)^{-2/3} (1 + \gamma_2 I_{\bar{C}_2}) (\mathbf{F}_1^{-T} : \delta \mathbf{F}_1) \mathbf{F}_1 (\mathbf{F}^*)^{-1} \quad (93) \\ & + \frac{2}{9} \alpha_2 e^{\gamma_2(I_{\bar{C}_2}-3)} I_{\bar{C}_2} (1 + \gamma_2 I_{\bar{C}_2}) (\mathbf{F}_1^{-T} : \delta \mathbf{F}_1) (\mathbf{F}^*)^T \mathbf{F}_1^{-T} \\ & - \frac{\alpha_2}{3} e^{\gamma_2(I_{\bar{C}_2}-3)} \left(\frac{J_1}{J^*}\right)^{-2/3} (1 + \gamma_2 I_{\bar{C}_2}) ((\mathbf{C}^*)^{-1} : \delta \mathbf{F}_1^T \mathbf{F}_1 \\ & + (\mathbf{C}^*)^{-1} : \mathbf{F}_1^T \delta \mathbf{F}_1) (\mathbf{F}^*)^T \mathbf{F}_1^{-T} \\ & + \alpha_2 \gamma_2 e^{\gamma_2(I_{\bar{C}_2}-3)} \left(\frac{J_1}{J^*}\right)^{-4/3} ((\mathbf{C}^*)^{-1} : \delta \mathbf{F}_1^T \mathbf{F}_1 \\ & + (\mathbf{C}^*)^{-1} : \mathbf{F}_1^T \delta \mathbf{F}_1) \mathbf{F}_1 (\mathbf{F}^*)^{-1} \\ & + \alpha_2 e^{\gamma_2(I_{\bar{C}_2}-3)} \left(\frac{J_1}{J^*}\right)^{-2/3} \delta \mathbf{F}_1 (\mathbf{F}^*)^{-1} \\ & + \frac{\alpha_2}{3} e^{\gamma_2(I_{\bar{C}_2}-3)} I_{\bar{C}_2} (\mathbf{F}^*)^T \mathbf{F}_1^{-T} \delta \mathbf{F}_1^T \mathbf{F}_1^{-T}. \end{aligned}$$

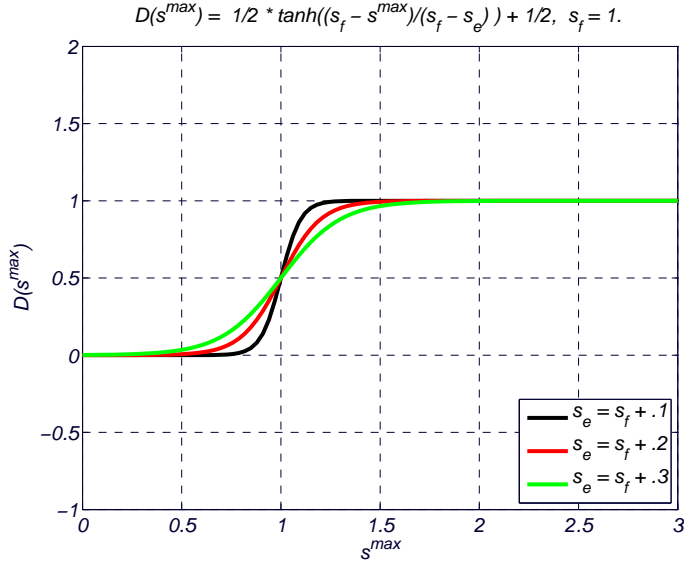


FIGURE 5: Example of analytic expression for the damage function $D(s^{max})$ for elastin degradation for different values of s_e .

2.5 Elastin degradation

The first mechanism is associated with the elastin component of arterial wall. As pointed out in Section 1.1, early stage aneurysm formation is hypothesized to be related to a mechanical damage of elastin. Hence, we introduce, in the multi-mechanism model a continuous isotropic damage model for the first mechanism. This approach, in the context of multi-mechanism models, was first presented by Robertson and coworkers [25].

We define an internal damage variable $D \in [0, 1]$ and following the approach described in [26] we postulate that the decoupled representation of the first mechanism strain energy function (see equation (34)) still holds for the *free energy*:

$$W_1^D(J, I_{\overline{C}_1}, II_{\overline{C}_1}, D) = W_{1vol}(J) + (1 - D)W_{1iso}(I_{\overline{C}_1}, II_{\overline{C}_1}), \quad (94)$$

where $W_{1vol}(J)$ is the same function defined in Section 2.3 which describes the volumetric elastic response, and $W_{1iso}(I_{\overline{C}_1}, II_{\overline{C}_1})$ is the isochoric effective strain energy of the undamaged material, which describes the isochoric elastic response. We observe that deformations due to temperature changes are neglected. As suggested in [27], the damage phenomenon affects only isochoric deformations. We call \mathbf{P}_1^D the first Piola-Kirchhoff stress tensor of the damage model.

From relation (94), the volumetric part of \mathbf{P}_1^D is

$$\mathbf{P}_{1vol}^D = \mathbf{P}_{1vol}, \quad (95)$$

and from the Clausius-Plank inequality, it follows that [28]:

$$\mathbf{P}_{1iso}^D = (1 - D)\mathbf{P}_{1iso}, \quad (96)$$

$$-\frac{\partial W_1^D}{\partial D}\dot{D} = W_{1iso}\dot{D} \geq 0. \quad (97)$$

Inequality (97) specifies that damage is a dissipative and irreversible phenomenon. Moreover, W_{1iso} is the thermodynamic conjugate variable of \dot{D} , and the evolution of D may be described in terms of W_{1iso} .

Let us consider again the scalar function of deformation $s(\bar{\mathbf{C}}_1(t))$ defined in (53), and consider a threshold s_b below which no damage occurs. We suppose that $s_b > s_a$, where s_a is defined in Section 2.4 and represents the scalar measure of deformation at which collagen is recruited. While the body deforms, as long as $s(\bar{\mathbf{C}}_1(t)) < s_b$, elastin damage never occurs and after the unloading stage the body recovers its initial stress-free configuration Ω_1 . Once the deformation threshold $s = s_b$ is reached, an irreversible damage to elastin component prevents the body, in the unloading stage, to recover the initial configuration Ω_1 and it will reach another stress-free configuration.

To take into account the gradual irreversible damage of elastin material, we define

$$s^{\max}(\bar{\mathbf{C}}_1(t)) = \max_{0 \leq \tau \leq t} s(\bar{\mathbf{C}}_1(\tau)), \quad (98)$$

as the maximum of our measure $s(\bar{\mathbf{C}}_1(t))$ during the history of deformation. At each time step, i.e. at each value of deformation, the quantity

$$\phi(\bar{\mathbf{C}}_1(t)) = s^{\max}(\bar{\mathbf{C}}_1(t)) - s(\bar{\mathbf{C}}_1(t)) = 0 \quad (99)$$

represents a surface in strain space. The normal to this surface is $\mathbf{N}_{iso} = \frac{\partial \phi}{\partial \bar{\mathbf{C}}_1}$; when $\mathbf{N}_{iso} : \delta \bar{\mathbf{C}}_1 > 0$ the strain is increasing (loading stage), otherwise when $\mathbf{N}_{iso} : \delta \bar{\mathbf{C}}_1 < 0$ the strain is decreasing (unloading stage).

An example of an analytic expression for the damage variable D in terms of s^{\max} is:

$$D(s^{\max}) = \frac{1}{2} \tanh \frac{s_f - s^{\max}(\bar{\mathbf{C}}_1(t))}{s_f - s_e} + \frac{1}{2}, \quad (100)$$

where s_f and s_e are two scalar parameters, and D depends on $\bar{\mathbf{C}}_1(t)$ through $s^{\max}(\bar{\mathbf{C}}_1(t))$. We observe that when $s^{\max} = s_f$, $D(s_f) = 0.5$, i.e. the elastin at the correspondent point is half-degraded, and s_e contains the information about the speed of the damage process.

At each time t , the evolution of the damage is regulated by

$$\dot{D} = \begin{cases} \frac{\partial D}{\partial s^{\max}} s^{\max} & \text{if } \phi = 0 \text{ and } \mathbf{N}_{iso} : \delta \bar{\mathbf{C}}_1 > 0, \\ 0 & \text{otherwise.} \end{cases} \quad (101)$$

Finally, we may represent the first Piola-Kirchhoff stress tensor \mathbf{P} of the full multi-mechanism model with damage as:

$$\mathbf{P} = \begin{cases} \mathbf{P}_{1vol} + \mathbf{P}_{1iso} & \text{for } 0 \leq s \leq s_a, \\ \mathbf{P}_{1vol} + \mathbf{P}_{1iso} + J^*(\mathbf{P}_{2vol} + \mathbf{P}_{2iso}) & \text{for } s_a < s \leq s_b, \\ \mathbf{P}_{1vol} + (1-D)\mathbf{P}_{1iso} + J^*(\mathbf{P}_{2vol} + \mathbf{P}_{2iso}) & \text{for } s > s_b. \end{cases} \quad (102)$$

As \mathbf{P}_{1vol} and \mathbf{P}_{2vol} have the role of penalizing the material compression, they do not have a specific constitutive meaning for the multi-mechanism model. Hence, to simplify the equation, we consider only one volumetric contribution:

$$\mathbf{P}_{vol} = \mathbf{P}_{1vol}, \quad (103)$$

and rewrite equation (102) as

$$\mathbf{P} = \mathbf{P}_{vol} + \begin{cases} \mathbf{P}_{1iso} & \text{for } 0 \leq s \leq s_a, \\ \mathbf{P}_{1iso} + J^*\mathbf{P}_{2iso} & \text{for } s_a < s \leq s_b, \\ (1-D)\mathbf{P}_{1iso} + J^*(\mathbf{P}_{2iso}) & \text{for } s > s_b. \end{cases} \quad (104)$$

From (64), the fourth order isochoric elasticity tensor for the first mechanism with damage is:

$$\mathbb{C}_{1iso}^D = \frac{\partial((1-D)\mathbf{P}_{1iso})}{\partial \mathbf{F}_1}, \quad (105)$$

and the linearization of the first Piola-Kirchhoff stress tensor reads

$$\mathbb{C}_{1iso}^D : \delta \mathbf{F}_1 = (1-D)\mathbb{C}_{1iso} : \delta \mathbf{F}_1 - \frac{\partial D}{\partial s}(\mathbf{P}_{1iso} \otimes \mathbf{P}_{1iso}) : \delta \mathbf{F}_1, \quad (106)$$

where $\mathbb{C}_{1iso} = \frac{\partial \mathbf{P}_{1iso}}{\partial \mathbf{F}_1}$ has been calculated in Section 2.4.2 in the case of a specific choice of a Neo-Hookean or exponential material for the first mechanism.

3 Weak formulation

In the Finite Element framework, we need to formulate the motion problem in a variational form and discretize it with respect to time and space. Our Finite Element discretization is quite standard, the main difficulty is in the calculation of the stress terms and their linearization.

We remark that non-linearity is an essential ingredient of elasticity for finite deformations. In finite elasticity, in general, the stress tensor depends upon non-linear kinematic terms that are a function of the deformation gradient. Moreover, if the constitutive law used to describe the material is a non-linear relation of stress and strain, the stress tensor is affected by another non-linearity. Another aspect of the formulation that increases the complexity of the computational problem is that the weak compressibility of the non-linear material of interest is manifested using a penalty term. This term is strongly non-linear with respect

to the deformation gradient by coupling all the components of the unknown displacement field.

The linearization, performed by computing the *Frechet* of the non-linear terms, and the solution of the system are obtained using an iterative Newton-Raphson procedure, enhanced with a linesearch backtracking algorithm.

The linearization of the nonlinear stress tensor needed in the Newton-Raphson method is the fourth order elasticity tensor. As described in Section 2.4.1, 2.4.2, and 2.5, we computed the exact form of the fourth order elasticity tensors for all the nonlinear materials introduced in the multi-mechanism model.

3.1 Principle of virtual power

Let us consider the bounded domain $\Omega_1 \subseteq \mathbb{R}^3$, representing the reference configuration of a body, the principle of virtual power may be expressed as:

$$\int_{\Omega_1} (\operatorname{div} \mathbf{P}(\mathbf{u}) + \rho_1 \mathbf{b} - \rho_1 \mathbf{a}) \cdot \delta \mathbf{v} \, d\Omega_1 = 0 \quad (107)$$

where $\delta \mathbf{v}$ is an arbitrary virtual velocity, satisfying possible constraints, the first Piola-Kirchhoff stress tensor \mathbf{P} is expressed as a function of unknown displacement $\mathbf{u} = \mathbf{u}(\mathbf{X}_1, t)$, $\mathbf{a} = \frac{D^2 \mathbf{u}}{Dt^2}$ is the acceleration field, and \mathbf{b} are the body forces.

The scalar equation (107) is fully equivalent to the vectorial motion equation:

$$\rho_1 \mathbf{a} = \operatorname{div} \mathbf{P}(\mathbf{u}) + \rho_1 \mathbf{b}, \quad (108)$$

thanks to the arbitrariness of the virtual velocity function. With further calculations we have:

$$\int_{\Omega_1} \rho_1 \frac{D^2 \mathbf{u}}{Dt^2} \cdot \delta \mathbf{v} \, d\Omega_1 = \int_{\Omega_1} \operatorname{div} \mathbf{P}(\mathbf{u}) \cdot \delta \mathbf{v} \, d\Omega_1 + \int_{\Omega_1} \rho_1 \mathbf{b} \cdot \delta \mathbf{v} \, d\Omega_1. \quad (109)$$

We define the external surface $\partial\Omega_1 = \Gamma_D \cup \Gamma_{N_0} \cup \Gamma_{N_t}$. In particular Γ_D is the part of the surface we impose the Dirichlet homogeneous boundary conditions and Γ_{N_0} , Γ_{N_t} are those parts where we prescribe the Newmann boundary conditions. Γ_{N_0} is the stress free surface and on Γ_{N_t} is imposed a known traction \mathbf{t} . The whole boundary conditions and initial values are:

$$\left\{ \begin{array}{l} \mathbf{u}(0) = \mathbf{u}_0; \\ \mathbf{v}(0) = \mathbf{v}_0; \\ \mathbf{u}(t) = \mathbf{0} \text{ on } \Gamma_D; \\ \mathbf{P}\mathbf{n} = \mathbf{0} \text{ on } \Gamma_{N_0}; \\ \mathbf{P}\mathbf{n} = \mathbf{t} \text{ on } \Gamma_{N_t}. \end{array} \right. \quad (110)$$

From the divergence theorem and the boundary conditions (110), we obtain:

$$\begin{aligned} \int_{\Omega_1} \rho_1 \frac{D^2 \mathbf{u}}{Dt^2} \cdot \delta \mathbf{v} \, d\Omega_1 = & - \int_{\Omega_1} \mathbf{P}(\mathbf{u}) : \nabla \delta \mathbf{v} \, d\Omega_1 \\ & + \int_{\partial\Omega_1} \mathbf{t} \cdot \delta \mathbf{v} \, d\Sigma_1 + \int_{\Omega_1} \rho_1 \mathbf{b} \cdot \delta \mathbf{v} \, d\Omega_1, \end{aligned} \quad (111)$$

where $d\Sigma_1$ is an infinitesimal surface element of $\partial\Omega_1$.

In particular, we observe that:

$$\nabla \delta \mathbf{v} = \frac{\partial}{\partial \mathbf{X}_1} \delta \mathbf{v} = \frac{\partial}{\partial \mathbf{X}_1} \frac{D \delta \boldsymbol{\eta}}{Dt} = \frac{D}{Dt} \frac{\partial \delta \boldsymbol{\eta}}{\partial \mathbf{X}_1} = \delta \dot{\mathbf{F}}_1, \quad (112)$$

with $\delta \boldsymbol{\eta}$ an arbitrary virtual displacement. The replacement of (112) in (111), gives the expression of the virtual power principle for the first Piola-Kirchhoff stress tensor \mathbf{P} with its conjugate virtual deformation $\delta \dot{\mathbf{F}}_1$:

$$\int_{\Omega_1} \rho_1 \frac{D^2 \mathbf{u}}{Dt^2} \cdot \delta \mathbf{v} \, d\Omega_1 + \int_{\Omega_1} \mathbf{P}(\mathbf{u}) : \delta \dot{\mathbf{F}}_1 \, d\Omega_1 = \int_{\partial\Omega_1} \mathbf{t} \cdot \delta \mathbf{v} \, d\Sigma_1 + \int_{\Omega_1} \rho_1 \mathbf{b} \cdot \delta \mathbf{v} \, d\Omega_1. \quad (113)$$

The reinterpretation of the virtual velocity $\delta \mathbf{v}$ in (113) as a test function, provides the weak formulation of problem (108).

3.2 Continuous weak formulation

Let V be the space of vector functions defined as follows:

$$V(\Omega_1) = \{\boldsymbol{\phi} \in [H^1(\Omega_1)]^3 \text{ such that } \boldsymbol{\phi} = \mathbf{0} \text{ on } \Gamma_D\}. \quad (114)$$

The weak formulation of problem (108) states:

For any $t > 0$ find $\mathbf{u} = \mathbf{u}(t) \in V(\Omega_1)$ such that $\mathbf{u}(0) = \mathbf{u}_0$, $\mathbf{v}(0) = \mathbf{v}_0$ and:

$$\int_{\Omega_1} \rho_1 \frac{D^2 \mathbf{u}}{Dt^2} \cdot \boldsymbol{\phi} \, d\Omega_1 + a(\mathbf{u}, \boldsymbol{\phi}) = \mathcal{F}(\boldsymbol{\phi}), \quad \forall \boldsymbol{\phi} \in V(\Omega_1) \quad (115)$$

with

$$a(\mathbf{u}, \boldsymbol{\phi}) = \int_{\Omega_1} \mathbf{P}(\mathbf{u}) : \nabla \boldsymbol{\phi} \, d\Omega_1, \quad (116)$$

and

$$\mathcal{F}(\boldsymbol{\phi}) = \int_{\partial\Omega_1} \mathbf{t} \cdot \boldsymbol{\phi} \, d\Sigma_1 + \int_{\Omega_1} \rho_1 \mathbf{b} \cdot \boldsymbol{\phi} \, d\Omega_1. \quad (117)$$

3.3 Discrete weak formulation

To perform the spatial discretization of equation (115), we consider the finite element spaces defined on a partition of the reference domain Ω_1 by a mesh τ_1^h made of generic elements K . Let us assume the mesh is geometrically conforming and made of tetrahedra. Hence, the approximated domain is

$$\Omega_1^h = \sum_{K \in \tau_1^h} K. \quad (118)$$

To perform the spatial discretization, we consider Lagrangian finite elements so that the corresponding functional space is:

$$\chi_N(\tau_1^h) = \{\phi_h \in C^0(\Omega_1^h), \phi_h|_K \in \mathbb{P}^N(K), \forall K \in \tau_1^h\}, \quad (119)$$

where $\mathbb{P}^N(K)$ is the space of polynomials of degree N defined on each element $K \in \tau_1^h$. The discrete functional space for the displacement unknown in the reference configuration is $V_h(\Omega_1^h) = [\chi_N(\tau_1^h)]^3$. Finally, the discrete weak formulation of the problem (115) can be written as:

For any $t > 0$ find $\mathbf{u}_h = \mathbf{u}_h(t) \in V_h(\Omega_1^h)$ such that $\mathbf{u}_h(0) = \mathbf{u}_{0h}$, $\mathbf{v}_h(0) = \mathbf{v}_{0h}$ and:

$$\int_{\Omega_1^h} \rho_1 \frac{D^2 \mathbf{u}_h}{Dt^2} \cdot \phi_h \, d\Omega_1 + a(\mathbf{u}_h, \phi_h) = \mathcal{F}(\phi_h), \quad \forall \phi_h \in V_h(\Omega_1^h) \quad (120)$$

with

$$a(\mathbf{u}_h, \phi_h) = \int_{\Omega_1^h} \mathbf{P}(\mathbf{u}_h) : \nabla \phi_h \, d\Omega_1, \quad (121)$$

and

$$\mathcal{F}(\phi_h) = \int_{\partial\Omega_1^h} \mathbf{t}_h \cdot \phi_h \, d\Sigma_1 + \int_{\Omega_1^h} \rho_1 \mathbf{b}_h \cdot \phi_h \, d\Omega_1, \quad (122)$$

where \mathbf{u}_{0h} and \mathbf{v}_{0h} are suitable approximation of the initial data compatible with the imposed boundary conditions; \mathbf{t}_h is an approximation of the imposed traction and \mathbf{b}_h is an approximation of the body forces.

Let $\{\phi_i\}_{i=1}^{N_V}$ be the Lagrange basis associated to the finite element space of displacement $V_h(\Omega_1^h)$, we approximate the solution as:

$$\mathbf{u}_h(\mathbf{X}) = \sum_{i \in N_V} \mathbf{u}_i \phi_i(\mathbf{X}) \quad (123)$$

The substitution of expression (123) in equation (120), supplies the algebraic form of the semi-discretized problem:

$$M\ddot{\mathbf{U}} + \mathbf{K}(\mathbf{U}) = \mathbf{F} \quad (124)$$

where \mathbf{U} is the unknown displacement vector. For a three-dimensional problem, if $\{\phi_i\}_{i=1}^{N_V}$ are linear functions, the size of vector \mathbf{U} is equal to the number of degrees of freedom, i.e. $3N_V$, where N_V is the number of nodes of the computational domain. M is the mass matrix and \mathbf{F} is the vector that takes into account the contributions of the body forces and the traction boundary condition. $\mathbf{K}(\mathbf{U})$ denotes a vector that takes into account the non-linear stiffness contribution due to the discretization of the stress tensors.

The representation of the generic entry (i, j) , with $i, j = \{1, \dots, N_V\}$ of each matrix and vector in system (124) is therefore:

$$M_{ij} = \int_{\Omega_1^h} \rho_1 \phi_i \phi_j \, d\Omega_1,$$

$$K(\mathbf{U})_j = \int_{\Omega_1^h} \mathbf{P}\left(\sum_{i \in N_V} \mathbf{U}_i \phi_i(\mathbf{X})\right) : \nabla \phi_j \, d\Omega_1,$$

$$F_j = \int_{\partial\Omega_1^h} \sum_{i \in N_V} t_i \phi_i \phi_j \, d\Sigma_1 + \int_{\Omega_1^h} \sum_{i \in N_V} b_i \phi_i \phi_j \, d\Omega_1.$$

3.4 Time Discretization

The initial-value problem for (124) consists of finding a displacement $\mathbf{U} = \mathbf{U}(t)$ satisfying (124) and the given initial data:

$$\mathbf{U}(0) = \mathbf{U}_0, \quad \dot{\mathbf{U}}(0) = \mathbf{V}_0. \quad (125)$$

To carry out the time discretization of system (124), we partition the time interval $\mathbb{I} = [0, T]$ into N subintervals $\mathbb{I}_n = [t^n, t^{n+1}]$, for $0 \leq n \leq N$, with $0 = t^0 < t^1 < \dots < t^N = T$, where t^n is a generic time step. For the sake of simplicity, we consider only uniform intervals $\delta t = \delta t_n = t^{n+1} - t^n$. In order to simplify the notation, we indicate with $\mathbf{U}^{n+1} = \mathbf{U}(t^{n+1})$ and similarly $\mathbf{F}^{n+1} = \mathbf{F}(t^{n+1})$.

Among all possible choices of time discretization schemes for a second order equation, we employ a *Newmark* scheme, which consists of the following equations:

$$M\mathbf{A}^{n+1} + \mathbf{K}(\mathbf{U}^{n+1}) = \mathbf{F}^{n+1}, \quad (126)$$

$$\mathbf{U}^{n+1} = \mathbf{U}^n + \delta t \mathbf{V}^n + \frac{\delta t^2}{2} [(1 - \zeta) \mathbf{A}^n + \zeta \mathbf{A}^{n+1}], \quad (127)$$

$$\mathbf{V}^{n+1} = \mathbf{V}^n + \delta t [(1 - \theta) \mathbf{A}^n + \theta \mathbf{A}^{n+1}], \quad (128)$$

where \mathbf{V}^{n+1} is the approximation of $\dot{\mathbf{U}}(t^{n+1})$ and \mathbf{A}^{n+1} is the approximation of $\ddot{\mathbf{U}}(t^{n+1})$ [29].

To guarantee the numerical stability of the scheme, the two parameters have to satisfy the relation $\theta \geq \frac{1}{2}$ and $\zeta \geq \frac{1}{2}(\theta + \frac{1}{2})^2$ [30]. The choice of parameters $\theta = \zeta = \frac{1}{2}$ leads to a second order method (mid-point), that is a fully non dissipative scheme, so that, no mechanism exists to damp high frequencies due to truncation errors [31].

In our case, we were interested in quasi-static deformations of the structures and, in order to avoid the spurious oscillations in the solution, we choose the parameters as $\theta = 0.5$ and $\zeta = 1$. With this choice, the time scheme reduces to the first order *Backward Euler* scheme for displacement equation, while for the velocity we still maintain the second order convergence [29]. The degradation of one order of the time scheme does not affect the precision of the displacement solution when looking for quasi-static deformations. In contrast, in the case of propagation of waves, the dynamics of the phenomenon is important and the precision of the time scheme becomes fundamental. With this in mind, the code was made to handle the general case so that these parameters could be selected depending on the application.

The use of scheme (126 – 128) in system (124) gives:

$$\frac{2}{\delta t^2} M \mathbf{U}^{n+1} + \zeta \mathbf{K}(\mathbf{U}^{n+1}) = \frac{2}{\delta t^2} M (\mathbf{U}^n + \delta t \mathbf{V}^n) + (1 - \zeta) M \mathbf{A}^n, \quad (129)$$

and

$$\mathbf{A}^{n+1} = \frac{2}{\zeta\delta t^2}\mathbf{U}^{n+1} - \frac{2}{\zeta\delta t^2}(\mathbf{U}^n + \delta t\mathbf{V}^n) - \frac{(1-\zeta)}{\zeta}\mathbf{A}^n, \quad (130)$$

$$\mathbf{V}^{n+1} = \mathbf{V}^n + \delta t[(1-\theta)\mathbf{A}^n + \theta\mathbf{A}^{n+1}]. \quad (131)$$

3.5 Linearization and solution

In this work the solution of the algebraic system (129) is performed iteratively using the *Newton-Raphson* method [22] [28].

Let us define the function $\mathcal{L}(\cdot) : \mathbb{R}^r \rightarrow \mathbb{R}^r$, where r is the total number of degrees of freedom, hence the dimension of system (129):

$$\begin{aligned} \mathcal{L}(\mathbf{U}^{n+1}) &= \frac{2}{\delta t^2}M\mathbf{U}^{n+1} + \zeta\mathbf{K}(\mathbf{U}^{n+1}) - \\ &\quad \frac{2}{\delta t^2}M(\mathbf{U}^n + \mathbf{V}^n\delta t) - (1-\zeta)M\mathbf{A}^n. \end{aligned} \quad (132)$$

With such an approach, solving system (129) is equivalent to finding the root of the nonlinear equation:

$$\mathcal{L}(\mathbf{U}^{n+1}) = 0 \quad (133)$$

Moreover, we observe that the term $-\frac{2}{\delta t^2}M(\mathbf{U}^n + \mathbf{V}^n\delta t) - (1-\zeta)M\mathbf{A}^n$ is a constant vector at each time step $n+1$, because it is computed by using the known vector \mathbf{U}^n . Let us consider the fixed time step t^{n+1} where we are computing the solution. Hence, the index k refers to a generic iteration of the Newton-Raphson method. Therefore we call $\mathbf{U}_k^{n+1} = \mathbf{U}_k$.

The general formulation of the Newton-Raphson method provides an iterative procedure to solve the nonlinear system (129). Given an initial guess \mathbf{U}_0 , at each iteration k we have to solve the linear system for the unknown $\delta\mathbf{U}_k = \mathbf{U}_{k+1} - \mathbf{U}_k$:

$$\mathcal{D}_{\mathbf{U}}\mathcal{L}(\mathbf{U}_k)[\delta\mathbf{U}_k] = -\mathcal{L}(\mathbf{U}_k). \quad (134)$$

After solving (134) in terms of $\delta\mathbf{U}_k$, we have to update the displacement $\mathbf{U}_{k+1} = \mathbf{U}_k + \delta\mathbf{U}_k$.

To solve (134) we need to compute the *Frechet* derivative or directional derivative of $\mathcal{L}(\mathbf{U}_k)$ with respect to an increment $\delta\mathbf{U}_k$ [32]:

$$\mathcal{D}_{\mathbf{U}}\mathcal{L}(\mathbf{U}_k)[\delta\mathbf{U}_k] = \lim_{\varepsilon \rightarrow 0} \frac{\mathcal{L}(\mathbf{U}_k + \varepsilon\delta\mathbf{U}_k) - \mathcal{L}(\mathbf{U}_k)}{\varepsilon}. \quad (135)$$

The displacement increment $\delta\mathbf{U}_k$ represents in \mathbb{R}^3 the direction along which we are differentiating the function \mathcal{L} . Referring to (132), we observe that

$$\mathcal{D}_{\mathbf{U}}\mathcal{L}(\mathbf{U}_k)[\delta\mathbf{U}_k] = \frac{2}{\delta t^2}M\delta\mathbf{U}_k + \zeta\mathcal{D}_{\mathbf{U}}\mathbf{K}(\mathbf{U}_k)[\delta\mathbf{U}_k], \quad (136)$$

hence the term to linearize is $\mathcal{D}_{\mathbf{U}}\mathbf{K}(\mathbf{U}_k)[\delta\mathbf{U}_k]$, that comes from the stress tensor. In order to understand how to perform the derivative of such a term, we recall that

$$\mathbf{K}(\mathbf{U}_k) = \int_{\Omega_1^h} \mathbf{P}(\mathbf{U}_k) : \nabla\phi \, d\Omega_1 \quad (137)$$

where \mathbf{P} is the first Piola-Kirchhoff stress tensor, nonlinear in \mathbf{U} , and ϕ is a test function defined in Section 3.3. As we pointed out above the linearization has to be performed at each iteration k of the Newton-Raphson method. To simplify the notation, in the following calculation we neglect the subscript k referred as the displacement vector \mathbf{U} and its variation $\delta\mathbf{U}$. We observe that integration in space on a fixed domain and functional derivation commute and from equation (137), we have

$$\begin{aligned} \mathcal{D}_{\mathbf{U}}\mathbf{K}(\mathbf{U})[\delta\mathbf{U}] &= \lim_{\varepsilon \rightarrow 0} \frac{1}{\varepsilon} \left(\mathbf{K}(\mathbf{U} + \varepsilon\mathbf{H}) - \mathbf{K}(\mathbf{U}) \right) = \\ &= \lim_{\varepsilon \rightarrow 0} \frac{1}{\varepsilon} \left(\int_{\Omega_1^h} \mathbf{P}(\mathbf{U} + \varepsilon\delta\mathbf{U}) : \nabla\phi \, d\Omega_1 - \int_{\Omega_1^h} \mathbf{P}(\mathbf{U}) : \nabla\phi \, d\Omega_1 \right) = \\ &= \int_{\Omega_1^h} \lim_{\varepsilon \rightarrow 0} \frac{1}{\varepsilon} \left(\mathbf{P}(\mathbf{U} + \varepsilon\delta\mathbf{U}) - \mathbf{P}(\mathbf{U}) \right) : \nabla\phi \, d\Omega_1 = \\ &= \int_{\Omega_1^h} \mathcal{D}_{\mathbf{U}}\mathbf{P}(\mathbf{U})[\delta\mathbf{U}] : \nabla\phi \, d\Omega_1. \end{aligned} \quad (138)$$

In particular, we observe that the first Piola-Kirchhoff stress tensor may depend on the unknown displacement \mathbf{U} through the deformation gradient \mathbf{F}_1 . In this case, we may employ the chain rule to linearize $\mathbf{P}(\mathbf{F}_1(\mathbf{U}))$:

$$\mathcal{D}_{\mathbf{U}}\mathbf{P}(\mathbf{F}(\mathbf{U}))[\delta\mathbf{U}] = \mathcal{D}_{\mathbf{F}_1}\mathbf{P}(\mathbf{F}_1)[\delta\mathbf{F}_1], \quad (139)$$

and

$$\mathcal{D}_{\mathbf{F}_1}\mathbf{K}(\mathbf{F}_1)[\delta\mathbf{F}_1] = \int_{\Omega_1^h} \mathcal{D}_{\mathbf{F}_1}\mathbf{P}(\mathbf{F}_1)[\delta\mathbf{F}_1] \, d\Omega_1. \quad (140)$$

It is useful to recall that, for a multi-mechanism model with weakly compressible materials (see section 2.3 and following), the most general expression of the nonlinear term $\mathbf{K}(\mathbf{F}_1)$ decomposes as

$$\mathbf{K}(\mathbf{F}_1) = \mathbf{K}_{1\,vol}(\mathbf{F}_1) + \mathbf{K}_{1\,iso}(\mathbf{F}_1) + \mathbf{K}_{2\,vol}(\mathbf{F}_1) + \mathbf{K}_{2\,iso}(\mathbf{F}_1), \quad (141)$$

where

$$\mathbf{K}_{l\,iso}(\mathbf{F}_1) = \int_{\Omega_1^h} \mathbf{P}_{l\,iso}(\mathbf{F}_1) : \nabla\phi \, d\Omega_1, \quad l = 1, 2; \quad (142)$$

$$\mathbf{K}_{l\,vol}(\mathbf{F}_1) = \int_{\Omega_1^h} \mathbf{P}_{l\,vol}(\mathbf{F}_1) : \nabla\phi \, d\Omega_1, \quad l = 1, 2. \quad (143)$$

3.5.1 Linesearch algorithm

Finally, we observe that the Newton-Raphson method is locally convergent, in the sense that it converges only if the initial guess is “close enough” to the solution. In order to improve the convergence properties and be independent from the initial guess, we add a *linesearch backtracking procedure* [33] to the basic algorithm. This technique consists in computing at each time step, a coefficient α_k to tune the descendent step computed by (134).

When the descendent direction $\delta\mathbf{U}_k$, is calculated according to (134), and \mathbf{U}_k is known, the coefficient α_k is computed as a minimum of $\mathcal{L}(\mathbf{U}_k + \alpha_k\delta\mathbf{U}_k)$:

$$\alpha_k = \arg \min_{\alpha \in \mathbb{R}^+} \mathcal{L}(\mathbf{U}_k + \alpha\delta\mathbf{U}_k) \quad (144)$$

In practical applications there are specific rules implemented to find α_k , we use the *Goldenstein Rules* [34].

The generic steps of the total algorithm can be summarized as follows:

1. Choose an initial guess \mathbf{U}_0 and a tolerance ε .
2. Compute a descendent direction $\delta\mathbf{U}_k$ solving (134).
3. Compute a suitable coefficient α_k through (144).
4. Update the solution $\mathbf{U}_{k+1} = \mathbf{U}_k + \alpha_k\delta\mathbf{U}_k$.
5. Test for convergence $\|\mathbf{U}_{k+1} - \mathbf{U}_k\| < \varepsilon$.
6. Exit if the test in 5. is true, go back to 2. if it is false.

4 Code validation, comparison with analytic solutions

The numerical code has been validated by comparing analytic solutions for a single mechanism material with numerical results for the same problem. The constitutive laws used in the validation procedure were a Neo-Hookean and exponential constitutive laws.

We consider a cylinder with axis in the x direction, with radius 0.5 cm and height 1 cm. The lower base of the cylinder is constrained to slide on the zy plane, so that it can shrink in direction orthogonal to its axis, but it can't move in the x direction (Dirichlet homogeneous boundary conditions on the x component of displacement). The upper section of the cylinder is loaded in traction. The lateral surface is stress free (Neumann homogeneous boundary conditions). The test is carried out as a series of quasi-static deformations and at each time step the traction increases linearly with time. A picture of results from the numerical simulation is shown in figure 6.

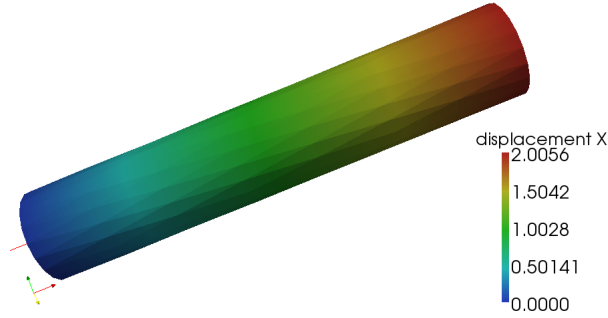


FIGURE 6: Example of the tension test carried on a cylinder with the isochoric Neo-Hookean constitutive law for a single-mechanism. The color scale represents the displacement in the axial direction (x).

4.1 Analytic solution

In the case of tension test of a cylinder loaded in the axial direction, the deformation λ_1 along the axis is homogeneous, and the corresponding first Piola-Kirchhoff stress tensor can be computed analytically. The deformation inside the cylinder is uniform. The axial direction and two orthogonal directions are principal axis of strain and stress, hence the deformation gradient \mathbf{F} is:

$$\mathbf{F} = \begin{pmatrix} \lambda_1 & 0 & 0 \\ 0 & \lambda_2 & 0 \\ 0 & 0 & \lambda_3 \end{pmatrix}, \quad (145)$$

where λ_2 and λ_3 are principal deformations in directions orthogonal to the axis. The jacobian of the motion is $J = \det \mathbf{F} = \lambda_1 \lambda_2 \lambda_3$.

The right Cauchy-Green strain tensor is:

$$\mathbf{C} = \begin{pmatrix} \lambda_1^2 & 0 & 0 \\ 0 & \lambda_2^2 & 0 \\ 0 & 0 & \lambda_3^2 \end{pmatrix}, \quad (146)$$

and from (30) the unimodular Cauchy-Green strain tensor $\overline{\mathbf{C}} = J^{-2/3} \mathbf{C}$.

The kinematics invariants we need, can be written in terms of principal stretches:

$$I_C = \text{tr} \mathbf{C} = \lambda_1^2 + \lambda_2^2 + \lambda_3^2; \quad (147)$$

$$I_{\overline{\mathbf{C}}} = \text{tr} \overline{\mathbf{C}} = J^{-2/3} I_C; \quad (148)$$

$$III_C = \det \mathbf{C} = J^2 = \lambda_1^2 \lambda_2^2 \lambda_3^2. \quad (149)$$

Because the test is symmetric in directions y and z , orthogonal to the axis x of the cylinder, we have that $\lambda_2 = \lambda_3$, and using relation (149) we find:

$$\lambda_2 = \lambda_3 = \sqrt{\frac{J}{\lambda_1}}. \quad (150)$$

The strain energy function W of the material is composed of a volumetric term (W_{vol}) depending only on J and a deviatoric term (W_{iso}) depending only on $I_{\overline{\mathbf{C}}}$, the first modified invariant of \mathbf{C} :

$$W = W_{iso}(I_{\overline{\mathbf{C}}}) + W_{vol}(J) \quad (151)$$

The first Piola-Kirchhoff stress tensor \mathbf{P} is obtained by evaluating $\frac{\partial W}{\partial \mathbf{F}}$. In the present simple case, from (44) the principal components of stress are:

$$P_{11} = 2 F_{11} \frac{\partial W}{\partial C_{11}}, \quad (152)$$

$$P_{22} = 2 F_{22} \frac{\partial W}{\partial C_{22}}, \quad (153)$$

$$P_{33} = 2 F_{33} \frac{\partial W}{\partial C_{33}}. \quad (154)$$

4.2 Neo-Hookean constitutive law

To represent the material behavior of the deviatoric part, we choose the Neo-Hookean constitutive law for a single-mechanism, given by (75), and for the volumetric part we use expression (67). In the paper of Neff and Hartmann [23] a proof of the polyconvexity of the chosen strain energy function that guarantees the existence of an equilibrium solution is shown.

After some calculations, the principal components of first Piola-Kirchhoff stress tensor are obtained:

$$P_{11} = \frac{\mu}{2} \left(\frac{2\lambda_1}{J^{2/3}} - \frac{2\lambda_2\lambda_3(\lambda_1^2 + \lambda_2^2 + \lambda_3^2)}{3J^{5/3}} \right) + \frac{K}{2\lambda_1} \ln J + \frac{K}{2} \lambda_2\lambda_3(J-1), \quad (155)$$

$$P_{22} = \frac{\mu}{2} \left(\frac{2\lambda_2}{J^{2/3}} - \frac{2\lambda_1\lambda_3(\lambda_1^2 + \lambda_2^2 + \lambda_3^2)}{3J^{5/3}} \right) + \frac{K}{2\lambda_2} \ln J + \frac{K}{2} \lambda_1\lambda_3(J-1), \quad (156)$$

$$P_{33} = \frac{\mu}{2} \left(\frac{2\lambda_3}{J^{2/3}} - \frac{2\lambda_1\lambda_2(\lambda_1^2 + \lambda_2^2 + \lambda_3^2)}{3J^{5/3}} \right) + \frac{K}{2\lambda_3} \ln J + \frac{K}{2} \lambda_1\lambda_2(J-1) \quad (157)$$

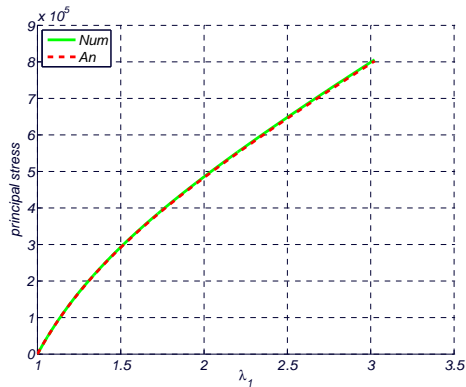
From (150), we can express λ_2 and λ_3 as function of J and λ_1 . As the lateral surface of the cylinder is stress free, $P_{22} = P_{33} = 0$. We can replace λ_2 and λ_3 , for example in equation (156), thus we obtain a relation between J and λ_1 :

$$P_{22} = \frac{\mu}{2} \left(\frac{2\sqrt{\frac{J}{\lambda_1}}}{J^{2/3}} - \frac{2\lambda_1\sqrt{\frac{J}{\lambda_1}}(\lambda_1^2 + 2\frac{J}{\lambda_1})}{3J^{5/3}} \right) + \frac{K}{2} \sqrt{\frac{\lambda_1}{J}} \ln J + \frac{K}{2} \lambda_1 \sqrt{\frac{J}{\lambda_1}} (J-1) = 0. \quad (158)$$

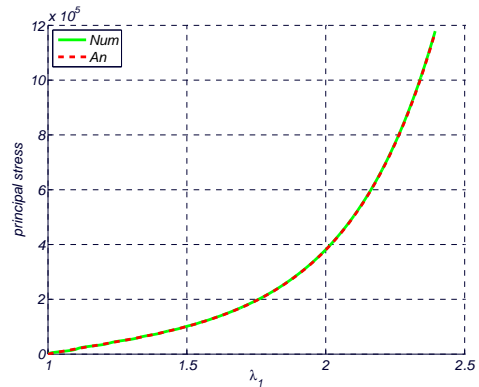
The solution of this algebraic equation gives J once the stretch λ_1 is fixed.

Finally we compute the principal component of stress in axial direction:

$$P_{11} = \frac{\mu}{2} \left(\frac{2\lambda_1}{J^{2/3}} - \frac{2J(\lambda_1^2 + 2\frac{J}{\lambda_1})}{3J^{5/3}} \right) + \frac{K}{2\lambda_1} \ln J + \frac{K}{2} \frac{J}{\lambda_1} (J-1). \quad (159)$$



(a) Analytic and numerical solution of the tension test with Neo-Hookean constitutive law.



(b) Analytic and numerical solution of the tension test with Exponential constitutive law.

FIGURE 7: Comparison between the analytic and the numerical solution. Both graphs represent the principal component P_{11} of the first Piola-Kirchhoff stress tensor versus the axial stretch λ_1 .

The technique used to derive the principal stress P_{11} follows that proposed in Ogden [35].

In Figure 7(a) the comparison between the analytic solution and the numerical solution of this tension test is shown. Material parameters are $\mu = 27.68 \cdot 10^5$ Pa and $K = 10^7$ Pa, for both the numerical and analytic solution.

4.3 Exponential constitutive law

In this section we use an exponential isochoric constitutive law to model a single-mechanism material. The corresponding strain energy function is given by expression (85). For the volumetric part of the strain energy function we again use (67). Also for the exponential case, in Neff and Hartmann [23] this choice of strain energy function is shown to be polyconvex, thus guaranteeing the existence of an equilibrium solution.

If we proceed with calculations as in the previous section, in this case, the

principal components of the first Piola-Kirchhoff stress tensor are:

$$\begin{aligned}
P_{11} &= \frac{\alpha}{2} \left(e^{\gamma \left(\frac{\lambda_1^2 + \lambda_2^2 + \lambda_3^2}{J^{2/3}} - 3 \right)} \left(\frac{2 \lambda_1}{J^{2/3}} - \frac{2 \lambda_2 \lambda_3 (\lambda_1^2 + \lambda_2^2 + \lambda_3^2)}{3 J^{5/3}} \right) \right) \\
&+ \frac{K}{2 \lambda_1} \ln J + \frac{K}{2} \lambda_2 \lambda_3 (J - 1), \tag{160}
\end{aligned}$$

$$\begin{aligned}
P_{22} &= \frac{\alpha}{2} \left(e^{\gamma \left(\frac{\lambda_1^2 + \lambda_2^2 + \lambda_3^2}{J^{2/3}} - 3 \right)} \left(\frac{2 \lambda_2}{J^{2/3}} - \frac{2 \lambda_1 \lambda_3 (\lambda_1^2 + \lambda_2^2 + \lambda_3^2)}{3 J^{5/3}} \right) \right) \\
&+ \frac{K}{2 \lambda_2} \ln J + \frac{K}{2} \lambda_1 \lambda_3 (J - 1), \tag{161}
\end{aligned}$$

$$\begin{aligned}
P_{33} &= \frac{\alpha}{2} \left(e^{\gamma \left(\frac{\lambda_1^2 + \lambda_2^2 + \lambda_3^2}{J^{2/3}} - 3 \right)} \left(\frac{2 \lambda_3}{J^{2/3}} - \frac{2 \lambda_1 \lambda_2 (\lambda_1^2 + \lambda_2^2 + \lambda_3^2)}{3 J^{5/3}} \right) \right) \\
&+ \frac{K}{2 \lambda_3} \ln J + \frac{K}{2} \lambda_1 \lambda_2 (J - 1). \tag{162}
\end{aligned}$$

As for the Neo-Hookean material, during the tension test, the lateral surface of the cylinder is stress free, and $P_{22} = P_{33} = 0$. If we consider equation $P_{22} = 0$ and we replace λ_2 and λ_3 by means of (150), we obtain a relation between J and λ_1 :

$$\begin{aligned}
P_{22} &= \frac{\alpha}{2} \left(e^{\gamma \left(\frac{\lambda_1^2 + 2 \frac{J}{\lambda_1}}{J^{2/3}} - 3 \right)} \left(\frac{2 \sqrt{\frac{J}{\lambda_1}}}{J^{2/3}} - \frac{2 \lambda_1 \sqrt{\frac{J}{\lambda_1}} (\lambda_1^2 + 2 \frac{J}{\lambda_1})}{3 J^{5/3}} \right) \right) \\
&+ \frac{K}{2} \sqrt{\frac{\lambda_1}{J}} \ln J + \frac{K}{2} \lambda_1 \sqrt{\frac{J}{\lambda_1}} (J - 1) = 0. \tag{163}
\end{aligned}$$

For a chosen λ_1 , we can compute J from (163) and the principal component of stress in the axial direction can be obtained from:

$$\begin{aligned}
P_{11} &= \frac{\alpha}{2} \left(e^{\gamma \left(\frac{\lambda_1^2 + 2 \frac{J}{\lambda_1}}{J^{2/3}} - 3 \right)} \left(\frac{2 \lambda_1}{J^{2/3}} - \frac{2 \frac{J}{\lambda_1} (\lambda_1^2 + 2 \frac{J}{\lambda_1})}{3 J^{5/3}} \right) \right) \\
&+ \frac{K}{2 \lambda_1} \ln J + \frac{K}{2} \frac{J}{\lambda_1} (J - 1), \tag{164}
\end{aligned}$$

As noted in Section 4.2, the technique used to derive the principal stress P_{11} follows the guideline proposed by Ogden [35].

In Figure 7(b) the analytic and the numerical solution for this tensions test are shown. The same material parameters have been used to compute the analytical solution and the numerical simulation. These are $\alpha_1 = 7.12 \cdot 10^3$ Pa, $\gamma_1 = 0.86$, and $K = 10^7$ Pa.

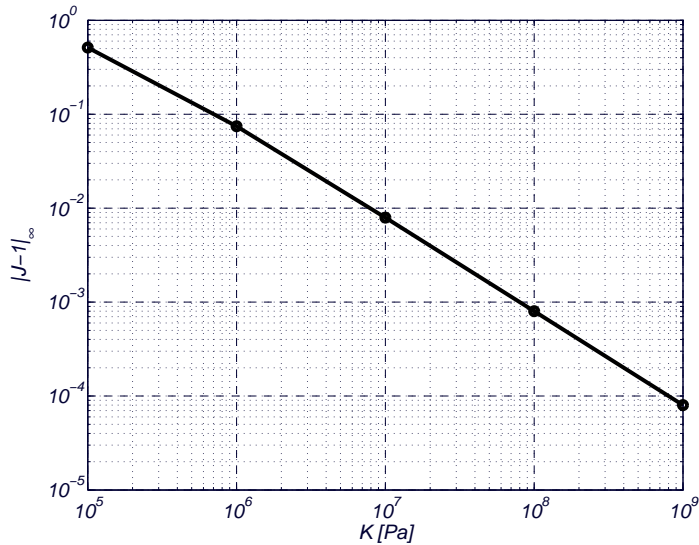


FIGURE 8: L_∞ norm of $(J - 1)$ with respect to different values of the bulk modulus K .

	Neo-Hook	Exponential
1 st Mech.	$\mu_1 = 27.68 \cdot 10^4$ Pa	$\alpha_1 = 7.12 \cdot 10^3$ Pa, $\gamma_1 = 0.86$
2 nd Mech.	-	$\alpha_2 = 31.28 \cdot 10^3$ Pa, $\gamma_2 = 1.87$

TABLE 1: Table of material parameters used in strain energy functions (67, 75, 85).

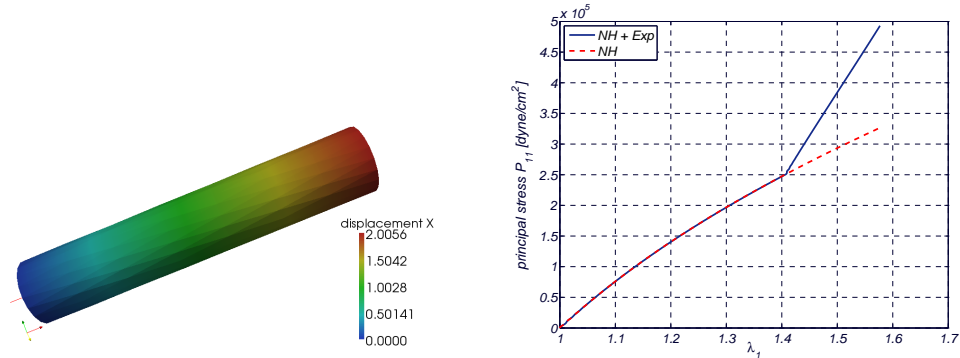
5 Material parameters

The strain energy function adopted herein is the sum of a Neo-Hookean material plus an Exponential law, for the second mechanism, as suggested in [24], [20]. The material parameters used for the double-mechanism are taken from the literature [20] and are listed in table 1.

The volumetric coefficient K (bulk modulus) of the strain energy function (see expression (67)) cannot be measured by experiments, it multiplies the volumetric part of the strain energy function, giving rise to a penalty term, that allows the material only slight compression. In Le Tallec [36], we find the suggestion that for a FE displacement formulation it should be in the range:

$$C_s \cdot 10^2 \leq K \leq C_s \cdot 10^6, \quad (165)$$

where C_s is the characteristic shear modulus of the material. For smaller values of K there is a loss of accuracy in computing the solution and for larger values the condition number of the associated discrete linear system becomes too large. In figure 8 is shown the relation between the compression modulus K and the compressibility the material exhibits when J moves away from 1.



(a) Example of the tension test carried on the cylinder with the isochoric Neo-Hookean constitutive law for a single-mechanism. The color scale represents the displacement in the axis direction (x). Scrolling is allowed on the lower base of the cylinder.

(b) Comparison between the stress-strain graph for the tension test with a single and a double mechanism law. The blue line is the behavior of a double Neo-Hook and Exponential model, and the red dashed line in a single Neo-Hookean model. The two curves overlap until the deformation threshold activates the exponential collagen mechanism.

FIGURE 9: Tension test in case of uniform deformations.

In this work we use for the bulk modulus the value $K = 10^7$ Pa, that is included in range (165) when $C_s = \mu_1$ or $C_s = \alpha_1$.

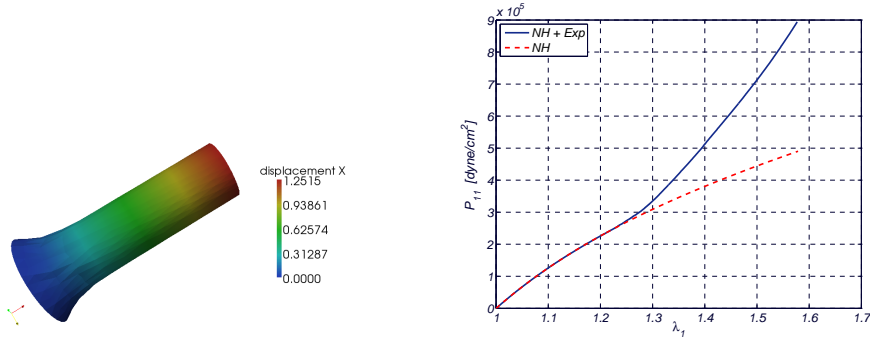
We observe that in [20] the chosen value of the compression modulus is $K = 10^9$ Pa, allowed by the use of a FE mixed (displacement and pressure) formulation.

6 Numerical results

Some simple numerical tests have been used to explain the behavior of the collagen recruitment mechanism within the double mechanism model in the case of uniform deformations and non-uniform deformations. The tests were performed as a series of quasi-static deformations.

We consider a cylinder with the upper surface in traction, linearly varying with time, the lateral surface is stress free, and the homogeneous Dirichlet boundary conditions are imposed on the component of displacement along the cylinder axis x on the lower surface. The initial length of the cylinder is 1 cm and its radius 0.5 cm. A picture of the deformed cylinder is shown in figure 9(a).

In this test, the deformation is uniform, i.e. it is the same at each point. Therefore, the deformation threshold $s_a = 0.5$ is reached simultaneously by all elements of the computational domain. In figure 9(b) a comparison of the stress-strain curve obtained with a double-mechanism and a single-mechanism model



(a) Example of a tension test carried on the cylinder with the isochoric Neo-Hookean constitutive law for a single-mechanism. The color scale represents the displacement in the axis direction (x). The lower base of the cylinder is now locked.

(b) Comparison between the stress-strain graph for a tension test with a single and a double mechanism law. The blue line is the behavior of a double Neo-Hookean and exponential model, and the red dashed line in a single Neo-Hookean model. The two curves smoothly separates because the collagen recruitment is gradual throughout the cylinder.

FIGURE 10: Tension test in case of non-uniform deformations.

is shown. The deformation λ_1 is computed as the current length over the initial length of the cylinder and the stress P_{11} is the principal first Piola-Kirchhoff stress component in the axial direction x . The double-mechanism, composed by a Neo-Hookean material for the first mechanism and an exponential material for the second, is compared with a single Neo-Hookean material. It can be observed, in figure 9(b), that the two curves overlap until the threshold value is reached (which corresponds to $s = s_a$). Above this value, they are different. In fact, at $s = s_a$ the second mechanism becomes active in all the points of the cylinder.

To test the behavior of the double-mechanism model for non-uniform deformation, we modify the previous tension test imposing a Dirichlet homogeneous boundary condition on all the components of displacement at the lower base of the cylinder (see figure 10(a)).

In this case, the deformation is not the same at all the points of the cylinder. As the deformation is non-uniform, at each time only some elements are activated. In figure 10(b) we plot P_{11} , the first Piola-Kirchhoff stress component in the axial direction x , versus the deformation λ_1 , computed as in the previous test. The blue curve represents a double-mechanism made of a Neo-Hookean and exponential material, and the red dashed curve is a single Neo-Hookean mechanism. In this case, we observe that before the collagen recruitment, the two curves overlap, but the split-up is very smooth, due to the fact that the second mechanism becomes active smoothly within the elements of the computational

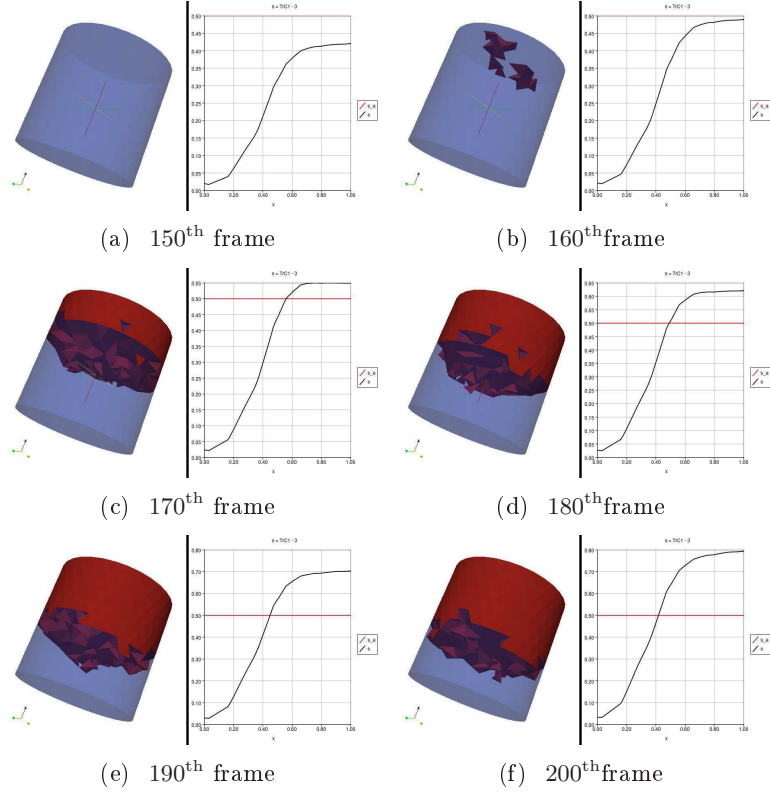


FIGURE 11: The picture shows the highlighting of activated elements at different time, i.e. at different values of traction, and the correspondent graph of scalar measure of deformation $s = \frac{1}{\mu_1} W_{1iso}^{NH}$, along the axis x , with respect to the activation threshold $s_a = 0.5$. The activated elements are plotted on the unloaded geometry.

domain.

We notice that for large enough traction, the deformation overcomes the threshold at the elements of the upper surface first, followed by the rest of the cylinder. Correspondingly, in figures 11, the activation of the elements belonging to the upper surface of the cylinder occurs earlier than the activation of the elements below them. In figures 11, activated elements at different time frame (i.e. at different values of traction) are shown highlighted on the unloaded geometry. Each picture is joined by the corresponding graph of the scalar measure of deformation $s = \frac{1}{\mu_1} W_{1iso}^{NH}$, defined in Section 2.4.2, along the cylinder axis x . The red horizontal line corresponds to $s = s_a = 0.5$.

6.1 Inflation of thick walled cylinder with narrowing radius

To show the behavior of the full multi-mechanism damage model, we consider an inflation test carried on a straight tube, representing a portion of an artery, where the inner radius is decreasing along the axis. This geometrical feature may represent an initial unhealthy situation of the artery.

The inflation test has been performed as a series of quasi static inflation, increasing the internal pressure linearly with time. The length of the tube is 3 cm, the minimum and maximum inner radius are 0.3 and 0.1 cm, and the outer radius is 0.5 cm. The parameters used are $s_a = 0.5$, for collagen activation, $s_e = 1.15$, and $s_f = 1.1$ for the elastin damage model. The geometrical domain used for the inflation test is made of 68973 tetrahedra.

The inflation of the cylinder induces a non-uniform deformation within the tube. In particular, the deformation is maximum at the inner of the cylinder and radially decreases toward the external surface. Hence, the activation of collagen elements starts from the elements belonging to the inner surface of the tube, where the activation threshold is overcome, and gradually involves contiguous elements.

Performing the test, we observe that the deformation field depends on the thickness of the tube. Where the arterial wall is thicker the deformation is smaller, and the subsequent activation of collagen involves only few elements close to the lumen, while where the wall is thinner, the deformation is larger and all the collagen elements are activated. In left figure 12, the elements in which collagen has been recruited are plotted on the unloaded geometry. The right figure 12 shows the elements in which the elastin is damaged. As for the collagen, we observe that where the arterial wall is thinner, the deformation is bigger and the damage of elastin elements happens earlier than in the rest of the tube, starting from the elements belonging to the lumen and propagating within the arterial wall.

We underline that the threshold for the irreversible damage of elastin is greater than the threshold for the collagen activation, i.e. the degradation of the first mechanism happens in the elements where the second mechanism is already present. From the point of view of the mechanical response of the material, this means that the elements where there is no more elastin are less stiff than the contiguous elements where both mechanisms are present.

In particular, this happens where the arterial wall is thinner. The consequence is that the arterial wall becomes weaker and consequently the deformation larger. In figure 13 we show the comparison between the unloaded geometry and the deformed geometry. In particular the deformation of the portion of the tube where the elastin is damaged may be very similar to the initial stage of an aneurysm formation. Let us suppose that the portion of the artery where the wall is thinner represents a pathological state, due to hemodynamical or geometrical factors. We may interpret our numerical results, as a prediction that, in presence of damage of elastin components, the portion of an artery where the

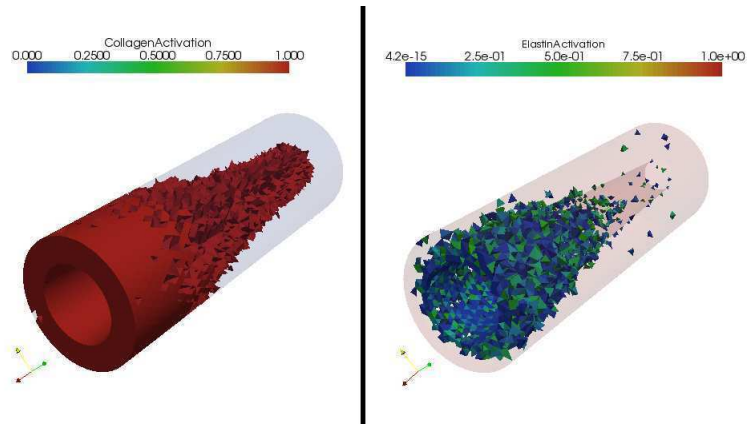


FIGURE 12: Picture of activated collagen elements (left) and damaged elastin elements (right) for an inflation test of a straight tube with narrowing radius. The final inflation pressure is 31 KPa. The activated and damaged elements are plotted on the unloaded geometry.

wall is thinner is very likely a site where an aneurysm will develop.

7 Conclusion and discussion

In this paper we have presented the numerical implementation and results obtained for a multi-mechanism model suitable to simulate the non-linear and inelastic behavior of cerebral arteries. The theoretical model was first presented by Robertson and coworkers [24].

The biggest challenge of this model is the need for two distinct reference configurations for elastin and collagen. Our contribution to the multi-mechanism model is the derivation of the Lagrangian formulation of the whole constitutive model in the first (elastin) reference configuration. Hence, it has been necessary to map the stress tensor of the collagen mechanism to the elastin reference configuration. The resulting non-standard formulation required particular attention in the code implementation. The final non-linear system has been solved by means of the Newton-Raphson method with exact jacobian computation [37]. The multi-mechanism model presented in this paper has been implemented in the Finite Element library LifeV [38].

The main limitation of the model presented is to consider the arterial wall homogeneous, while its real structure is layered and each layer is characterized by a strong anisotropy due to a particular orientation of collagen fibers. Moreover we can underline that the modular procedure used to define the strain energy function can easily be extended to the anisotropic case as shown in [20], [25].

Even with such limitation, the numerical results obtained with our solver show that the multi-mechanism model is able to capture the non-linear char-

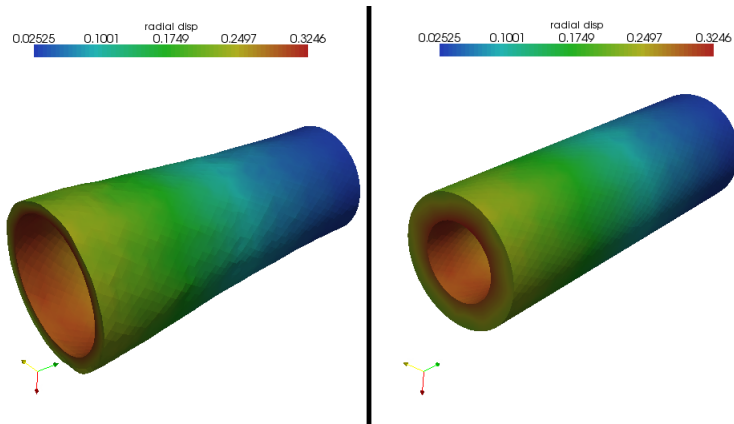


FIGURE 13: Comparison between the unloaded geometry and the deformed geometry of a portion of a cylindrical artery with inner narrow radius. In particular the deformation of the portion of the tube where the elastin is damaged may be very similar to the initial stage of an aneurysm formation.

acteristics of the arterial wall. At low levels of deformation the elastin (first mechanism) supplies weak resistance to the tension test, while when the collagen enters the model, it renders the whole material stiffer, until the elastin damage occurs. We showed that the way the collagen is recruited depends in a very general way by the deformation field.

We observed that in presence of a non-uniform deformation field, within the computational domain, we may have some elements in which only the first mechanism is active, elements in which both first and second mechanism are present, and elements in which the second mechanism is active and the first is totally or partially damaged. Regarding a single element, the collagen activation and the elastin degradation are implemented as gradual phenomena, that do not induce a discontinuity in the stress tensor governing the mechanical response of the specific element. But contiguous elements may have different and discontinuous stress response, and such a phenomenon may induce instabilities in the whole material behavior. This difficulty is overcome by using a well refined mesh.

Finally a more realistic inflation test has been shown. In this numerical simulation, we observe that the collagen recruitment and elastin deactivation start from the lumen of the arteries, where the deformation is wider. In particular, the narrowing of the internal radius of the cylinder, may be interpreted as an initial unhealthy situation, that leads to a non-uniform damage of the elastin mechanism and leads to an enlargement of the arterial segment. From a qualitative point of view the enlargement may represent the initial stage of an aneurysm formation, due to mechanical damage of elastin components of arterial wall.

References

- [1] J. L. Brisman, J. K. Song, and D. W. Newell. Cerebral aneurysms. *The New England Journal of Medicine*, 335:928–939, 2006.
- [2] M. El Khaldi, P. Pernter, F. Ferro, A. Alferi, N. Decaminada, L. Naibo, and G Bonatti. Detection of cerebral aneurysms in nontraumatic subarachnoid haemorrhage: role of multislice ct angiography in 130 consecutive patients. *Radiol. Med.*, 112:123–137, 2007.
- [3] J. J. Provencio and N. Vora. Subarachnoid hemorrhage and inflammation: bench to bedside and back. *Semin Neurol*, 25(4):435–444, Dec 2005.
- [4] T. Willis. *Cerebri Anatome*. Londinii, 1664.
- [5] R. W. Thompson. Basic science of abdominal aortic aneurysms: emerging therapeutic strategies for an unresolved clinical problem. *Current Opinion in Cardiology*., 11(5):455–557, 1996.
- [6] J. A. G. Rhodin. Architecture of the vessel wall. *Handbook of Physiology, The Cardiovascular System*, 2:1–31, 1980.
- [7] O. E. Idowu, M. T. Shokunbi, A. O. Malom, and E. E. U. Akang. Anomalies, aneurysm and histology of the middle cerebral artery in nigerian africans. *Int. J. Morphol.*, 26(4):1023–1027, 2008.
- [8] W. E. Stehbens. Histopathology of cerebral aneurysms. *Arch Neurol.*, 8(3):272–285, 1963.
- [9] R. Wulandana. *A Nonlinear and Inelastic Constitutive Equation for Human Cerebral Arterial and Aneurysm Wall*. PhD thesis, University of Pittsburgh, 2003.
- [10] J. Frösen, A. Piippo, A. Paetau, M. Kangasniemi, M. Niemelä, J. Hernesniemi, and J. Jääskeläinen. Remodeling of saccular cerebral artery aneurysm wall is associated with rupture. *Stroke*, 35:2287–2293, 2004.
- [11] G. A. Holzapfel and T. C. Gasser. A new constitutive framework for arterial wall mechanics and a comparative study of material models. *Journal of Elasticity*, 61:1–48, 2000.
- [12] S. Scott, G. G. Ferguson, and M. Roach. Comparison of the elastic properties of human intracranial arteries and aneurysms. *J Physiol Pharmacol*, 50:328–332, 1972.
- [13] National institute of neurosurgical disorders and stroke, <http://www.ninds.nih.gov>.

- [14] C. Vega, J. V. Kwon, and S. D. Lavine. Intracranial aneurysms: Current evidence and clinical practice. *American Family Physician*, 2002.
- [15] International study of unruptured intracranial aneurysms, <http://www.isuia.org>.
- [16] G. W. Britz, L. Salem, D. W. Newell, J. Eskridge, and D. R. Flum. Impact of surgical clipping on survival in unruptured and ruptured cerebral aneurysms: a population-based study. *Stroke*, 35(6):1399–1403, Jun 2004.
- [17] S. I. Stiver, P. J. Porter, R. A. Willinsky, and M. C. Wallace. Acute human histopathology of an intracranial aneurysm treated using Guglielmi detachable coils: case report and review of the literature. *Neurosurgery*, 43(5):1203–1208, Nov 1998.
- [18] T. Nakagawa and K. Hashi. The incidence and treatment of asymptomatic, unruptured cerebral aneurysms. *J Neurosurg*, 80(2):217–223, 1994.
- [19] K. Matsumoto. Investigation of the surgically treated and untreated unruptured cerebral aneurysms of the anterior circulation. *Surgical Neurology*, 60(6):516–522, 2003.
- [20] D. Li and A. M. Robertson. A structural multi-mechanism constitutive equation for cerebral arterial tissue. *International Journal of Solids and Structures*, 46:2920–2928, 2009.
- [21] S. K. Kyriacou and J. D. Humphrey. Influence of size, shape and properties on the mechanics of axisymmetric saccular aneurysms. *J Biomech*, 29(8):1015–1022, Aug 1996.
- [22] J. Bonet and R. D. Wood. *Nonlinear Continuum Mechanics for Finite Element Analysis*. Cambridge University Press, 1997.
- [23] P. Neff and S. Hartman. Polyconvexity of generalized polynomial-type hyperelastic strain energy functions for near-incompressibility. *International Journal of Solids and Structures*, 40:2767–2791, 2003.
- [24] R. Wulandana and A. M. Robertson. An inelastic multi-mechanism constitutive equation for cerebral arterial tissue. *Biomech. Model. Mechanobiol.*, 4(4):235–248, Dec 2005.
- [25] D. Li and A. M. Robertson. A structural multi-mechanism damage model for cerebral arterial tissue. *J. Biomech. Eng.*, 131(10):101013.1–101013.8, 2009.
- [26] J. F. Rodriguez, V. Alastrue, and M. Doblare. Finite element implementation of a stochastic three dimensional finite-strain damage model for fibrous soft tissue. *Comput. Appl. Mech. Engrg.*, 197:946–958, 2008.

- [27] J. C. Simo. On a fully three-dimensional finite-strain viscoelastic damage model: Formulation and computational aspects. *Computer Methods in Applied Mechanics and Engineering*, 60(2):153–173, 1987.
- [28] G. A. Holzapfel. *Nonlinear Solid Mechanics: A Continuum Approach for Engineering*. Wiley, John & Sons, Incorporated, 2000.
- [29] Thomas J. R. Hughes. *The finite element method*. Prentice-Hall, 1987.
- [30] A. Quarteroni, R. Sacco, and F. Saleri. *Numerical Mathematics*. Springer, 2000.
- [31] A. Quarteroni and A. Valli. *Domain Decomposition Methods for Partial Differential Equations*. Oxford University Press, Oxford, 1999.
- [32] P. G. Ciarlet. *Mathematical Elasticity*. Elsevier Science Publisher B.V., 1988.
- [33] P. Brown and Y. Saad. Hybrid krylov methods for nonlinear system of equations. *SIAM Journal Science and Statistical Computing*, 11:450–481, 1990.
- [34] A. A. Goldstein. On steepest descent. *SIAM Journal on Control*, 3:147–151, 1965.
- [35] R. W. Ogden. *Non-Linear Elastic Deformations*. John Wiley and Sons, 1984.
- [36] P. Le Tallec. Numerical methods for nonlinear three dimensional elasticity. In *Handbook of Numerical Analysis, VOL III*. Elsevier Science, 1994.
- [37] M. de Luca. *Mathematical and Numerical Models for Cerebral Aneurysm Wall Mechanics*. PhD thesis, Politecnico di Milano, 2009.
- [38] <http://www.lifev.org/>.

MOX Technical Reports, last issues

Dipartimento di Matematica “F. Brioschi”,
Politecnico di Milano, Via Bonardi 9 - 20133 Milano (Italy)

- 25/2011** DE LUCA, M.; AMBROSI, D.; ROBERTSON, A.M.; VENEZIANI, A.; QUARTERONI, A.
Finite element analysis for a multi-mechanism damage model of cerebral arterial tissue
- 24/2011** MANZONI, A.; QUARTERONI, A.; ROZZA, G.
Model reduction techniques for fast blood flow simulation in parametrized geometries
- 23/2011** BECK, J.; NOBILE, F.; TAMELLINI, L.; TEMPONE, R.
On the optimal polynomial approximation of stochastic PDEs by Galerkin and Collocation methods
- 22/2011** AZZIMONTI, L.; IEVA, F.; PAGANONI, A.M.
Nonlinear nonparametric mixed-effects models for unsupervised classification
- 21/2011** AMBROSI, D.; PEZZUTO, S.
Active stress vs. active strain in mechanobiology: constitutive issues
- 20/2011** ANTONIETTI, P.F.; HOUSTON, P.
Preconditioning high-order Discontinuous Galerkin discretizations of elliptic problems
- 19/2011** PASSERINI, T.; SANGALLI, L.; VANTINI, S.; PICCINELLI, M.; BACIGALUPPI, S.; ANTIGA, L.; BOCCARDI, E.; SECCHI, P.; VENEZIANI, A.
An Integrated Statistical Investigation of the Internal Carotid Arteries hosting Cerebral Aneurysms
- 18/2011** BLANCO, P.; GERVASIO, P.; QUARTERONI, A.
Extended variational formulation for heterogeneous partial differential equations
- 17/2011** QUARTERONI, A.; ROZZA, G.; MANZONI, A.
Certified Reduced Basis Approximation for Parametrized Partial Differential Equations and Applications
- 16/2011** MESIN, L.; AMBROSI, D.
Spiral waves on a contractile tissue